

NASICON-Structured Materials for Energy Storage

Zelang Jian, Yong-Sheng Hu, Xiulei Ji,* and Wen Chen*

The demand for electrical energy storage (EES) is ever increasing, which calls for better batteries. NASICON-structured materials represent a family of important electrodes due to its superior ionic conductivity and stable structures. A wide range of materials have been considered, where both vanadium-based and titanium-based materials are recommended as being of great interest. NASICON-structured materials are suitable for both the cathode and the anode, where the operation potential can be easily tuned by the choice of transition metal and/or polyanion group in the structure. NASICON-structured materials also represent a class of solid electrolytes, which are widely employed in all-solid-state ion batteries, all-solid-state air batteries, and hybrid batteries. NASICON-structured materials are reviewed with a focus on both electrode materials and solid-state electrolytes.

1. Introduction

Renewable energy is pivotal for the sustainable prosperity of our society. Advanced energy-storage technologies will be the enabler for intermittent energy sources, such as wind and solar power.^[1] Rechargeable metal-ion batteries represent the state of the art of energy-storage devices.^[2] To build powerful batteries, a great number of electrode materials have been investigated. With respect to cathodes, most cathode materials can be classified into two categories: close-packed metal oxide structures, such as layered oxides,^[3] and more-open three-dimensional (3D) framework structures, such as polyanionic compounds.^[4] One well-known example of the latter group is NASICON (NAtrium Super Ionic CONductor)-structured materials.^[5]

Dr. Z. Jian, Prof. W. Chen
State Key Laboratory of Advanced Technology
for Materials Synthesis and Processing School
of Materials Science and Engineering
Wuhan University of Technology
Wuhan 430070, China
E-mail: chenw@whut.edu.cn

Dr. Z. Jian, Prof. X. Ji
Department of Chemistry
Oregon State University
Corvallis, OR 97331-4003, USA
E-mail: David.Ji@oregonstate.edu

Prof. Y.-S. Hu
Key Laboratory for Renewable Energy
Beijing Key Laboratory for New Energy, Materials and Devices
Beijing National Laboratory for Condensed Matter Physics
Institute of Physics
Chinese Academy of Sciences
Beijing 100190, China

DOI: 10.1002/adma.201601925



NASICON-structured materials are particularly attractive because they exhibit great structural stability, as well as fast ionic conductivity. The first known NASICON was $\text{Na}_{1+x}\text{Zr}_x\text{P}_{3-x}\text{Si}_x\text{O}_{12}$ ($0 \leq x \leq 3$), which is a typical solid electrolyte.^[6] The NASICON structure has the formula of $\text{A}_x\text{MM}'(\text{XO}_4)_3$, where MO_6 and $\text{M}'\text{O}_6$ octahedra share all their corners with XO_4 tetrahedra. Octahedral MO_6 and $\text{M}'\text{O}_6$ connect with three tetrahedral XO_4 units, which constitutes a basic unit, and is named a lantern. Each lantern joins six other lanterns, generating a large interstitial space that can accommodate 0 to 5 alkali cations per structural formula. The number of alkali cations depends on the oxidation states of M and M' and the X element. In NASICON-structured materials, some possible elements are as follows:

- i) A = Li, Na, K, Mg, Ca;
- ii) M or M' = Fe, V, Ti, Zr, Sc, Mn, Nb, In;
- iii) X = S, P, Si, As.

NASICON compounds of the same composition may exhibit different crystal structures, i.e., rhombohedral (r-) and monoclinic (m-) structures, as shown in Figure 1a,b. For the rhombohedral structure, the M–M' dimers ($[\text{MO}_6]_2[\text{XO}_4]_3$) are well aligned along the c -axis (Figure 1c), whereas the M–M' dimers of the monoclinic structure display a zigzag alignment (Figure 1d). Therefore, the same composition may present different electrochemical behaviors because of the different structures.

Before NASICON was considered as an insertion host for alkali ions, there was a long research history of over 10 years on the study of these materials as solid electrolytes.^[7] In the NASICON-type structure, lithium ions or sodium ions can be facilely inserted and extracted. Considering the rapidly growing demand for large-scale energy-storage applications, the development of new batteries based on earth-abundant elements provides more-sustainable solutions. Therefore, due to the abundant resources of sodium and its low cost, increasing attention has been focused on sodium-ion batteries (NIBs). Here, we review NASICON materials for NIBs, as well as lithium-ion batteries (LIBs).

Although several reviews have been published on electrode materials or solid-state electrolytes, which includes progress of the NASICON-structured materials to some extent,^[5a,8] no review to date has been dedicated to systematically describing the development of NASICON-structured materials for energy storage. This review fills this gap by covering electrode materials and solid electrolytes for LIBs, NIBs, metal-air batteries, and new battery systems.

2. Electrode Materials

2.1. Iron-Based Materials

Although the NASICON structure was first identified from $\text{Na}_{1+x}\text{Zr}_2\text{P}_{3-x}\text{Si}_x\text{O}_{12}$, this structure can accommodate other ions, such as Li^+ and Mg^{2+} , thus being promising as electrode materials for LIBs or magnesium-ion batteries (MIBs).^[9] Iron-based electrode materials are very attractive due to their abundant resources and low cost. Iron-based NASICON-structured materials for lithium insertion were reported in pioneering works by Nadiri,^[10] Reiff,^[11] Torardi,^[12] and Manthiram^[13] on $\text{Li}_x\text{Fe}_2(\text{MO}_4)_3$ ($\text{M} = \text{Mo}, \text{W}$). The chemical method (by reaction with a calculated amount of n-butyllithium diluted with dry petroleum spirit) was employed to achieve the lithium insertion into the NASICON framework, where they determined the lithium-storage mechanism as being a two-phase reaction between the monoclinic structure ($\text{Fe}_2(\text{MO}_4)_3$) and the orthorhombic structure ($\text{Li}_2\text{Fe}_2(\text{MO}_4)_3$). The operation voltage is ≈ 3.0 V vs Li^+/Li , which corresponds to the $\text{Fe}^{3+}/\text{Fe}^{2+}$ redox couple.^[13]

Manthiram et al. demonstrated excellent reversibility of lithium storage in m- $\text{Fe}_2(\text{SO}_4)_3$,^[14] which shows a flat plateau at 3.6 V vs Li^+/Li , corresponding to the $\text{Fe}^{3+}/\text{Fe}^{2+}$ redox couple, which is 0.6 V higher than that of the same redox couple in $\text{Fe}_2(\text{MoO}_4)_3$ or $\text{Fe}_2(\text{WO}_4)_3$. This is clear evidence of the inductive effect of the element "X" in the XO_4 groups. The operation voltage depends on the electronegativity of X, where S (VI) exhibits stronger electron-withdrawing capability than Mo (VI) or W (VI), thus weakening the M-O bands and raising the operation voltage of the same redox couple. Manthiram et al. also investigated the lithium-storage properties of r- $\text{Fe}_2(\text{SO}_4)_3$, which shows a slope instead of a plateau in the potential profiles.^[14] Okada et al. studied the lithium-storage behavior of m- $\text{Li}_3\text{Fe}_2(\text{PO}_4)_3$,^[15] Masquelier et al.^[16] and Morcrette et al.^[17] further reported the electrochemical performance of $\text{Li}_3\text{Fe}_2(\text{PO}_4)_3$ with different structures, where r- $\text{Li}_3\text{Fe}_2(\text{PO}_4)_3$ presents a slope, whereas m- $\text{Li}_3\text{Fe}_2(\text{PO}_4)_3$ exhibits two plateaus (Figure 2). Padhi et al. tuned the potentials of the redox couples in NASICON materials by anionic substitution of XO_4 .^[18] r- $\text{Li}_3\text{Fe}_2(\text{PO}_4)_3$ displays a slope with an average potential of 2.8 V vs Li^+/Li , in which the position of the $\text{Fe}^{3+}/\text{Fe}^{2+}$ redox couple was substantially shifted by 0.8 V when switching from S to P. r- $\text{LiFe}_2(\text{SO}_4)_2(\text{PO}_4)$ displays a slope with an average voltage of ≈ 3.3 V vs Li^+/Li , which is between those of $\text{Li}_3\text{Fe}_2(\text{PO}_4)_3$ and $\text{Fe}_2(\text{SO}_4)_3$ for lithium storage (Figure 3). Masquelier et al. also investigated the lithium storage in r- $\text{Li}_3\text{Fe}_2(\text{AsO}_4)_3$ and m- $\text{Li}_3\text{Fe}_2(\text{AsO}_4)_3$.^[16] Both materials exhibit two sequential plateaus with different potentials. The plateaus are located at 2.9, 2.6, and 3.1, 2.4 V vs Li^+/Li in the discharge curves of r- $\text{Li}_3\text{Fe}_2(\text{AsO}_4)_3$ and m- $\text{Li}_3\text{Fe}_2(\text{AsO}_4)_3$, respectively.

The sodium-storage behaviors in iron-based NASICON materials have been investigated as well. Bruce et al. studied reversible sodium intercalation into $\text{Fe}_2(\text{MoO}_4)_3$ or $\text{Fe}_2(\text{WO}_4)_3$, yielding two new compounds, $\text{Na}_2\text{Fe}_2(\text{MoO}_4)_3$ or $\text{Na}_2\text{Fe}_2(\text{WO}_4)_3$, which retain the monoclinic symmetry.^[19] Both electrodes show the voltage of 2.7 V vs Na^+/Na , which is 0.3 V lower than their lithium counterparts. The Li- and Na-storage behavior in $\text{Fe}_2(\text{MoO}_4)_3$ is shown in Figure 4.^[13,19] This disparity comes from the difference between the potentials of Li^+/Li and



Zelang Jian received his M.Sc. degree (2010) from Wuhan University of Technology. He completed his Ph.D. degree in 2012 at Wuhan University of Technology and the Institute of Physics, Chinese Academy of Sciences. He then joined Prof. Haoshen Zhou's group at the National Institute of Advanced Industrial Science

and Technology (AIST). After several months in Prof. Yan Yao's group at the University of Houston, he moved to Prof. Xiulei Ji's group at Oregon State University. He is currently working on advanced materials for stationary energy storage, including new materials for sodium/potassium-ion batteries, and energy storage mechanism.



Xiulei Ji received his B.Sc. degree from Jilin University in 2003, supervised by Professor Bai Yang. In 2009, he obtained his Ph.D. degree working in Professor Linda F. Nazar's group at the University of Waterloo. From 2010 to 2012, he was an NSERC Postdoctoral Fellow, advised by Professor Galen D. Stucky at the University of California, Santa Barbara. Since 2012, he has been an Assistant Professor of Chemistry at Oregon State University. His current research interests are the exploration of basic materials chemistry of carbon-based materials for energy purposes.



Wen Chen is a professor and Ph. D supervisor at the State Key Laboratory of Advanced Technology for Materials Processing, Wuhan University of Technology. He received his Ph.D. degree in materials science in 1998 from Wuhan University of Technology. He is a director of the Chinese Solid Ion Association. His research area mainly covers the structure of functional materials and physical effects.

Na^+/Na redox couples as they are counter/reference electrodes, indicating that the $\text{Fe}^{3+}/\text{Fe}^{2+}$ redox couple operates in the same manner. Sun et al. fabricated m- $\text{Fe}_2(\text{MoO}_4)_3$ film by magnetron sputtering as a cathode in NIBs, which shows much better cycling life than a bulk material.^[20] Recently, Nguyen et al. synthesized composites of $\text{Fe}_2(\text{MoO}_4)_3$ and conductive materials,

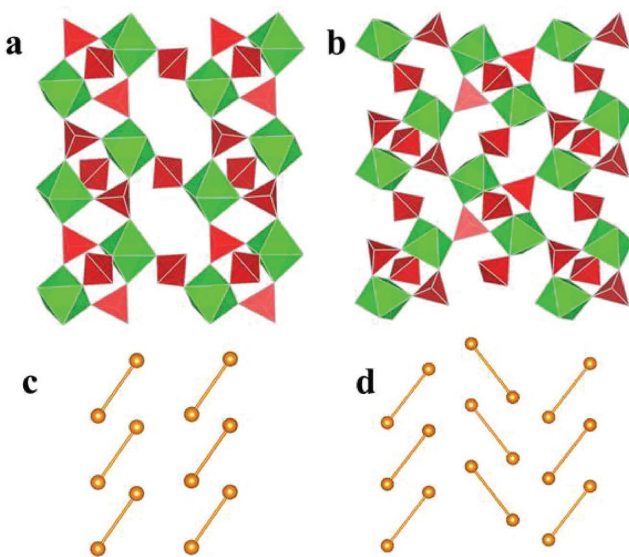


Figure 1. a–d) Schematic diagrams of rhombohedral structure (a,c) and monoclinic structure (b,d).

such as silver, carbon nanotubes, and reduced graphene oxide, which exhibit greatly improved cycling stability as cathodes for NIBs.^[21]

Iron-based NASICON cathodes have been developed for LIBs or NIBs with storage capacity of $\approx 120 \text{ mA h g}^{-1}$, corresponding to two-electron transfer (i.e., 2Li or 2Na insertion per formula (where $\text{Fe}_2(\text{MoO}_4)_3$ is one formula)).^[13,14,18] The operation voltage of the $\text{Fe}^{3+}/\text{Fe}^{2+}$ redox couple depends on the Li^+ /Li or Na^+ /Na redox couple and the Fe–O bond strengths, which can be adjusted by X elements.

2.2. Vanadium-Based Materials

Vanadium can give a series of redox couples: $\text{V}^{5+}/\text{V}^{4+}$, $\text{V}^{4+}/\text{V}^{3+}$, and $\text{V}^{3+}/\text{V}^{2+}$, which can result in multi-electron transfer.^[22] Therefore, vanadium-based NASICON materials can supply a high capacity. For example, $\text{Li}_3\text{V}_2(\text{PO}_4)_3$ as a cathode exhibits a capacity of 197 mA h g^{-1} .^[8a,23] Furthermore, both $\text{V}^{5+}/\text{V}^{4+}$ and $\text{V}^{4+}/\text{V}^{3+}$ couples show high operation potentials. The potential

of $\text{V}^{3+}/\text{V}^{2+}$ is low, and this couple can be used as anode materials.^[24] Recently, vanadium-based NASICON materials have been becoming a hot topic for energy storage.

$\text{V}_2(\text{SO}_4)_3$ occurs in either rhombohedral or monoclinic form, in which a pure monoclinic phase cannot be formed and is always mixed with the rhombohedral phase.^[25] The electrochemical behavior of $\text{V}_2(\text{SO}_4)_3$ shows two steps located at 2.63 and 2.59 V vs Li⁺/Li, corresponding to the $\text{V}^{3+}/\text{V}^{2+}$ redox couple. X-ray diffraction (XRD) results reveal the complex lithium-storage mechanism.

Attention to vanadium-based NASICON materials for energy storage is mainly focused on their phosphates. The thermodynamically stable $\text{Li}_3\text{V}_2(\text{PO}_4)_3$ (LVP) is of the monoclinic form.^[26] Three Li⁺ ions occupy different lattice sites, where Li1 is located at the tetrahedral site, and Li2 and Li3 occupy different pseudotetrahedral sites (Figure 5). All three Li⁺ ions are mobile, leading to a high theoretical capacity of 197 mA h g^{-1} .^[27]

With different cut-off potential ranges, m-LVP displays different potential profiles (Figure 6).^[8a] In the range of 3.0–4.8 V vs Li⁺/Li, four plateaus are located at 3.6, 3.7, 4.1, and 4.6 V vs Li⁺/Li during the charge process, corresponding to extraction of the first 0.5 Li⁺ ion, another 0.5 Li⁺ ion, and a second, and a third Li⁺ ion from m-LVP, respectively. In the discharge process, one long slope and two short plateaus are displayed, which can be assigned to the reversible process with the two Li⁺ ions, 0.5 Li⁺ ions, and 0.5 Li⁺ ions re-inserted, respectively.^[28] In the charge process, four plateaus correspond to four two-phase reactions; while in the discharge process, the slope represents a single-phase reaction, and the two small plateaus are for two two-phase reactions.^[29] When the cut-off voltage range is narrowed to 3.0–4.3 V vs Li⁺/Li, m-LVP shows a series of three obvious two-phase transitions in both the charging and the discharge processes, where there is no slope. The volume shrinks by $\approx 6.8\%$ ^[30] from $\text{Li}_3\text{V}_2(\text{PO}_4)_3$ to $\text{LiV}_2(\text{PO}_4)_3$, and then slightly decreases by 7.8%^[27] upon further oxidation to $\text{V}_2(\text{PO}_4)_3$.

Although different diffusion coefficient values of Li⁺ ions in m-LVP have been reported, they were mostly at the order of $10^{-9} \text{ cm}^2 \text{ s}^{-1}$, which is higher than that of LiFePO_4 or Li-rich layered oxides. It is still relatively low, due to the long diffusion distance of lithium for micrometer-sized materials. The low intrinsic diffusion coefficient can be enhanced by element doping,^[31] whereas the Li⁺ ion diffusion length can be shortened by decreasing the particle size.^[29b,32] The intrinsic

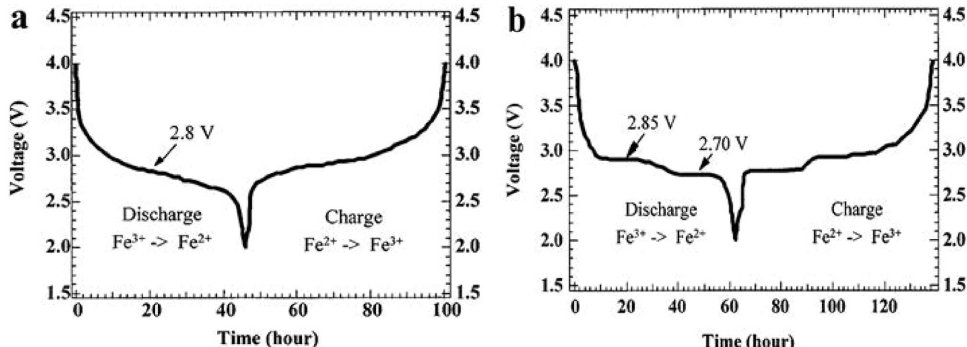


Figure 2. a,b) Discharge/charge curves of r- $\text{Li}_3\text{Fe}_2(\text{PO}_4)_3$ (a) and m- $\text{Li}_3\text{Fe}_2(\text{PO}_4)_3$ (b) for the first cycle at 0.1 mA cm^{-2} . Reproduced with permission.^[16] Copyright 1998, Elsevier.

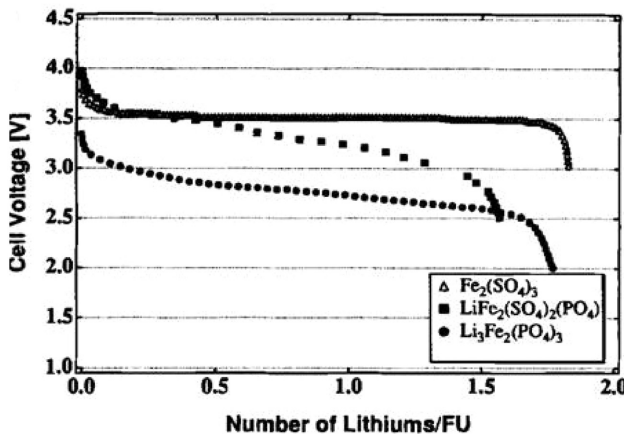


Figure 3. Discharge curves of r-Li₃Fe₂(PO₄)₃, r-LiFe₂(SO₄)₂(PO₄), and r-Fe₂(SO₄)₃ at a current density of 0.05 mA cm⁻². Reproduced with permission.^[18] Copyright 1998, The Electrochemical Society.

electronic conductivity in m-LVP is $\approx 10^{-8}$ S cm⁻¹,^[27,33] which is fairly low and comparable to that of LiFePO₄^[34] due to the insulating nature of phosphates.^[35] Doping with transition metals can increase the intrinsic electronic conductivity as well, and carbon coating can increase the surface conductivity.^[13,33]

The particle size of materials prepared by solid-state reactions is relatively large (ca. 5 μ m), resulting in poor electrochemical performance, especially low rate capability.^[36] The sol-gel method was carried out to synthesize carbon-coated and nanostructured m-LVP, which greatly improves the performance.^[23,29b,37] Many other methods have been employed to prepare m-LVP.^[38] Duan et al. obtained carbon-coated LVP with a small particle size of \approx 30 nm by a hydrothermal method,^[39] which delivered a reversible capacity of 138 mA h g⁻¹ with capacity retention of 86% after 1000 cycles at 5C in a cut-off range of 3–4.8 V vs Li⁺/Li. Chen et al. synthesized nanofibers with a diameter of 200 nm, which exhibited a capacity of 190 and 132 mA h g⁻¹ at 0.1C and 20C, respectively, between 3.0 and 4.8 V vs Li⁺/Li.^[40] Rui et al. obtained

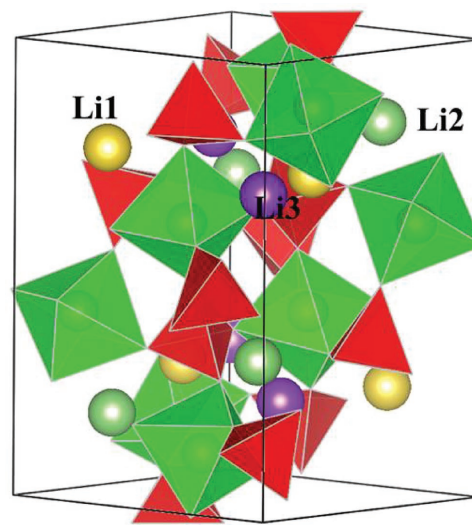


Figure 5. Schematic crystal structure of m-LVP.

LVP nanocrystals (5–8 nm) embedded in a nanoporous carbon matrix attached onto reduced graphene oxide (rGO) nanosheets.^[41] The composite presents high capacities, stable cycling life and excellent rate capability, where the capacity can reach 90 mA h g⁻¹ at 50C between 3.0 and 4.3 V, and remains at 88 mA h g⁻¹ after 1000 cycles. Wei et al. designed hierarchical-carbon-coated m-LVP mesoporous nanowires that showed a high capacity of 117 mA h g⁻¹ at 10C and excellent cycling stability of 80% capacity retention over 3000 cycles at 5C between 3.0 and 4.3 V vs Li⁺/Li.^[42] Proposed by Chung et al., doping can improve the intrinsic electronic conductivity and Li⁺-ion diffusivity of phosphates.^[35] Along this line, Na⁺,^[43] Mg²⁺,^[31,44] Ni²⁺,^[45] Al³⁺,^[46] Cr³⁺,^[47] Ti⁴⁺,^[48] Zr⁴⁺,^[49] and Mo⁶⁺^[50] have been used as dopants to improve the electrochemical performance in m-LVP system. For example, Cho et al. reported that carbon-supported and Al-doped m-LVP presents excellent rate performance at 20C between 3.0 and 4.8 V vs Li⁺/Li with a capacity of \approx 120 mA h g⁻¹ over 100 cycles.^[46b]

The redox couples of V⁵⁺/V⁴⁺ and V⁴⁺/V³⁺ facilitate LVP as a cathode, while the redox couple of V³⁺/V²⁺ enables LVP to operate as an anode as well. Rui et al. demonstrated that in m-LVP, two Li⁺ ions can be inserted with four plateaus at 1.9, 1.8, 1.7, and 1.6 V in the voltage range of 3.0–1.0 V vs Li⁺/Li (Figure 7), and two more Li⁺ can be further inserted, where Li₇V₂(PO₄)₃ is formed with the cut-off voltage going down to 0 V Li⁺/Li.^[24a] Kobayashi et al. fabricated a symmetric solid-state battery with m-LVP as both cathode and anode, which delivered capacities of 92 mA h g⁻¹ at 80 °C and 38 mA h g⁻¹ at 25 °C at 22 μ A cm⁻².^[51] Mao et al. assembled symmetric LVP cells that presented a 2.2 V operation potential and a high capacity of 162 mA h g⁻¹ (based on cathode mass).^[52]

As another type of LVP, rhombohedral LVP cannot be directly obtained in a direct synthetic way, but can be formed by ion exchange on the more thermodynamically stable sodium counterpart—Na₃V₂(PO₄)₃ (NVP).^[53] Therefore, r-LVP has the same structure as r-NVP (we will introduce the structural details below in Section 2.2 discussing NVP). Gaubicher et al. demonstrated that two lithium ions can be extracted from the r-LVP

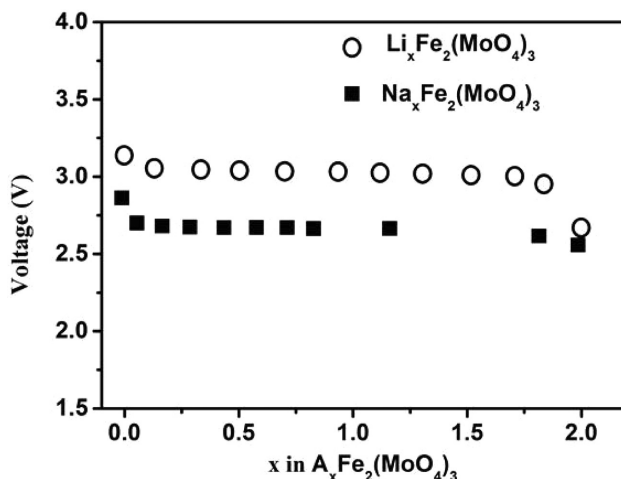


Figure 4. Li- and Na-storage behavior in Fe₂(MoO₄)₃.

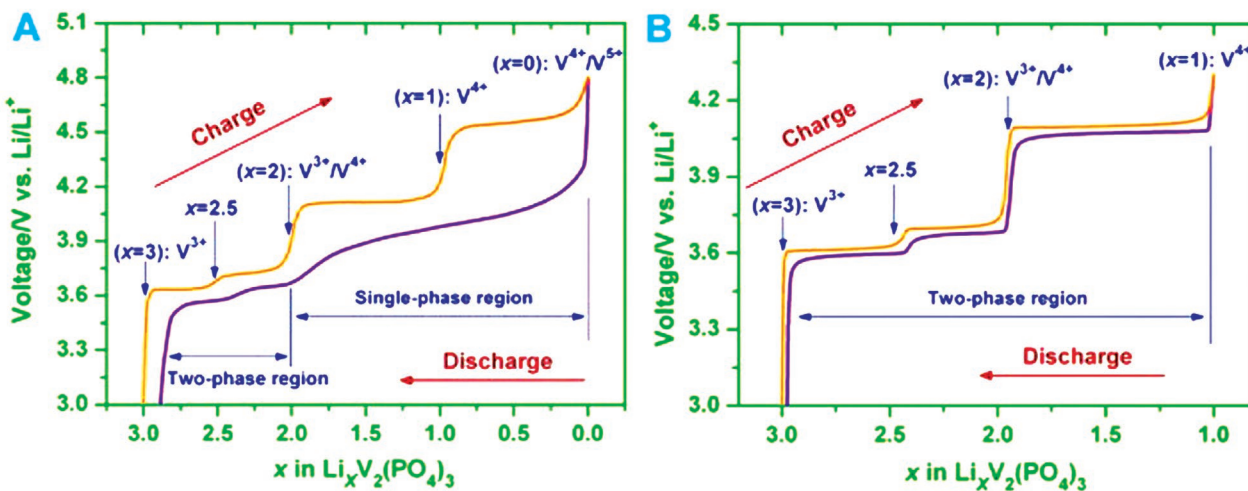


Figure 6. The electrochemical voltage–composition curves of m- $\text{Li}_3\text{V}_2(\text{PO}_4)_3$ in the voltage ranges of 3.0–4.8 V (A) and 3.0–4.3 V (B) vs Li^+/Li . Reproduced with permission.^[8a] Copyright 2014, Elsevier.

unit at ≈ 3.7 V vs Li^+/Li .^[53a] Morcrette et al. studied the structural evolution of r-LVP and m-LVP.^[30] Lithium extraction from r-LVP leads to r- $\text{LiV}_2(\text{PO}_4)_3$, indicating a two-phase reaction. Cushing et al. obtained $\text{Li}_2\text{NaV}_2(\text{PO}_4)_3$ via ion exchange, which also shows a 3.7 V vs Li^+/Li plateau. The Na^+ ions tend to remain immobilized, suggesting a Li-ion transport mechanism.^[54] Lu et al. presented that the r- $\text{Li}_1\text{V}_{1.9}\text{Al}_{0.1}(\text{PO}_4)_3$ has a more stable structure and much better rate performance, compared to r-LVP.^[55] Jian et al. prepared carbon-coated r-LVP, where two Li^+ ions can be extracted and two more Li^+ ions can be inserted into the structure, corresponding to $\text{V}^{3+}/\text{V}^{4+}$ with a plateau at 3.75 V and $\text{V}^{3+}/\text{V}^{2+}$ with an average potential of 1.75 V vs Li^+/Li , respectively. A symmetric full-cell battery was fabricated, showing a high capacity with an operation voltage of 2.0 V.^[56]

NVP has also attracted great attention for NIBs. As the cathode for NIBs, NVP shows a high operation potential of

3.4 V vs Na^+/Na and a high capacity of 117 mA h g^{-1} .^[57] In addition, the $\text{V}^{3+}/\text{V}^{2+}$ redox couple makes NVP a good anode.

The thermodynamically stable phase of NVP is rhombohedral,^[57a,58] which is different to its lithium counterpart.^[26] The crystal structure of NVP was first specified as the rhombohedral ($\text{R}\bar{3}\text{c}$) phase by Delmas et al. in 1978.^[59] Three Na^+ ions have two different sites (Figure 8), where one Na^+ ion (Na1) is in the 6b sites (six-coordinate Na–O sites), and the other two Na^+ ions reside in the 18e sites (eight-coordinate Na–O sites).^[60] However, Masquelier and co-workers recently argued that NVP adopts the monoclinic form at low temperatures (i.e., $< 25.8^\circ\text{C}$); a complex forms at a middle-range temperature and then transforms to rhombohedral at high temperatures ($> 177.2^\circ\text{C}$).^[61] Others reported that NVP adopts rhombohedral symmetry.^[53a,54,58b,59,62] The difference may lie in the different synthetic processes or particle size or carbon-coating effect. Here, we will focus on the electrochemical performance of rhombohedral NVP since the electrochemical performance of monoclinic NVP has not been reported.

Plashnitsa et al. introduced NVP as the electrodes for NIBs, where two plateaus ($\text{V}^{4+}/\text{V}^{3+}$ and $\text{V}^{3+}/\text{V}^{2+}$ redox couples) and poor cycling performance were reported in a symmetric full-cell.^[57a] Jian et al. first reported carbon-coated NVP, which shows a plateau anodic behavior at 3.4 V and a cathodic profile at 1.6 V vs Na^+/Na , corresponding to $\text{V}^{4+}/\text{V}^{3+}$ and $\text{V}^{3+}/\text{V}^{2+}$ redox couples, respectively.^[57b] As the cathode and anode, NVP delivers capacities of 98.6 and 66 mA h g^{-1} , respectively, which indicates that about two Na^+ ions can be extracted from NVP (forming $\text{NaV}_2(\text{PO}_4)_3$), or that one more Na^+ ion can be inserted into the NVP structure (forming $\text{Na}_4\text{V}_2(\text{PO}_4)_3$). Jian et al. further observed the insertion of a fifth Na^+ ion into NVP, which presents a plateau at 0.3 V vs Na^+/Na .^[63] The typical charge/discharge curves are shown in Figure 9a. Three plateaus can be observed, which corresponds to the extraction of two Na^+ ions at 3.4 V vs Na^+/Na , one Na^+ -ion insertion at 1.6 V Na^+/Na , and one more Na^+ -ion insertion at 0.5 V vs Na^+/Na , respectively. The corresponding cyclic voltammetry (CV) curve is shown in Figure 9b, revealing three reversible redox couples.

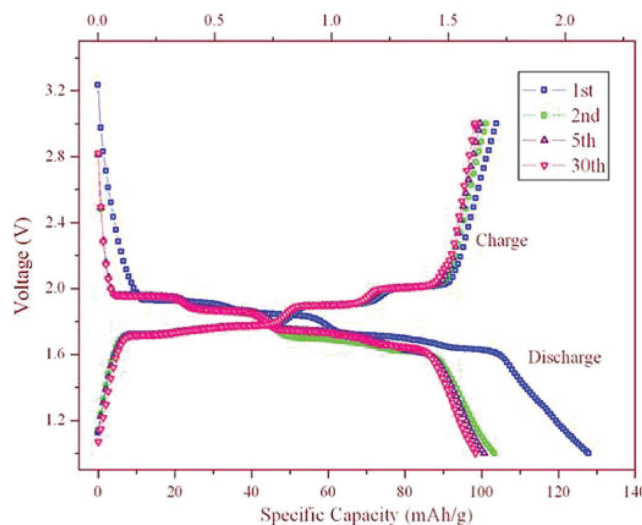


Figure 7. Discharge/charge profiles of LVP at a current density of 0.013 mA cm^{-2} in the voltage region of 3.0–1.0 V. Reproduced with permission.^[24a] Copyright 2011, Elsevier.

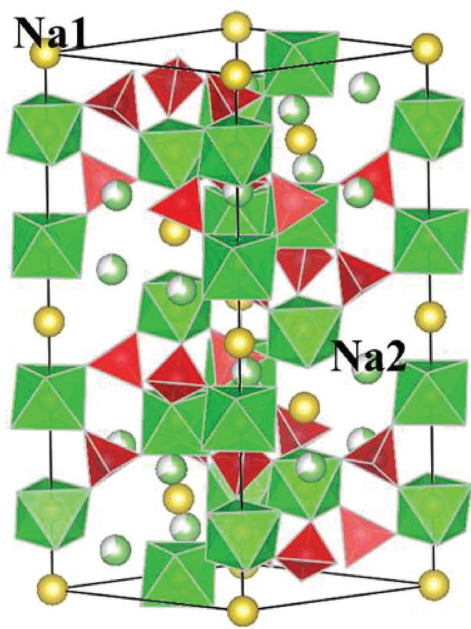


Figure 8. Schematic diagrams of NVP.

To understand the sodium-storage mechanism in NVP as the cathode, *in situ* XRD (Figure 10), spherical-aberration-corrected transmission electron microscopy (TEM) (Figure 11), and solid-state NMR have been employed.^[60,64] The results indicate that it is a typical two-phase reaction. There are three Na⁺ ions per NVP unit, and only two of them can be extracted.^[60,64,65] Two removable Na⁺ ions are located at the 18e site, where 2/3 of the vacancy is orderly occupied. The third Na⁺ ion occupies the 6b site, which cannot be extracted from the NVP structure.^[60] The two-phase reaction between NVP and NaV₂(PO₄)₃ corresponds to a volume change of 8.26%,^[64] close to that of LiFePO₄.^[66] By the chemical method, only two Na⁺ ions were pulled out, forming NaV₂(PO₄)₃, which confirms the electrochemical

results.^[60] Although Gopalakrishnan et al. reported that rhombohedral V₂(PO₄)₃ can be obtained from NVP, detailed experimental details were not provided.^[58a]

Carbon coating greatly enhances the capacity, cycling performance, and high-rate performance of NVP.^[68] Saravanan et al. prepared porous carbon-coated NVP, which presented a capacity of 116 mA h g⁻¹ and 50% capacity retention after 30 000 cycles at 40C. It also exhibited excellent rate performance, where the capacity could reach 91 and 62 mA h g⁻¹ at 20C and 40C, respectively.^[69] Li et al. synthesized NVP nanograins dispersed in different carbon matrices.^[70] NVP in activated carbon delivers a high capacity of 117.5 mA h g⁻¹ at 0.5C. Fang et al. synthesized a hierarchical and highly conductive carbon framework to coat and interconnect NVP particles, which demonstrated a close-to-theory reversible capacity at 0.2C (115 mA h g⁻¹).^[71] The composite presented a superior high-rate capability (38 mA h g⁻¹ at 500C), and an ultralong cycling stability (54% capacity retention after 20 000 cycles at 30C). Zhu et al. reported that 3D NVP:rGO-CNT (reduced graphene oxide–carbon nanotube) framework was directly deposited on the current collector.^[72] The composite exhibits a capacity of 109 mA h g⁻¹ at 30C and could reach 82 mA h g⁻¹ at 100C (in only 36 s). After 2000 cycles at 10C, 96% of the original capacity could be retained (Figure 12a,b).

NVP has also been widely studied as the anode for NIBs, particularly in symmetric batteries, where both the anode and the cathode are NVP.^[57a] Zhu et al. demonstrated that NVP as the anode shows a high capacity and stable cycling as 3D NVP:rGO-CNT (Figure 12c,d).^[72] A symmetric battery was assembled, which delivered a high capacity of 90 mA h g⁻¹ (based on the cathode mass) with an operation voltage at 1.7 V at 10C (Figure 12e,f). Duan et al. demonstrated that an NVP@C (carbon) core–shell nanocomposite exhibited a higher capacity as the cathode than pure NVP and bulk NVP@C.^[73] The symmetric full-cell showed a capacity of 90.9 mA h g⁻¹ and an energy density of ≈154.5 Wh kg⁻¹ (based on the cathode mass). Jian et al. investigated a symmetric Na-ion pseudocapacitor

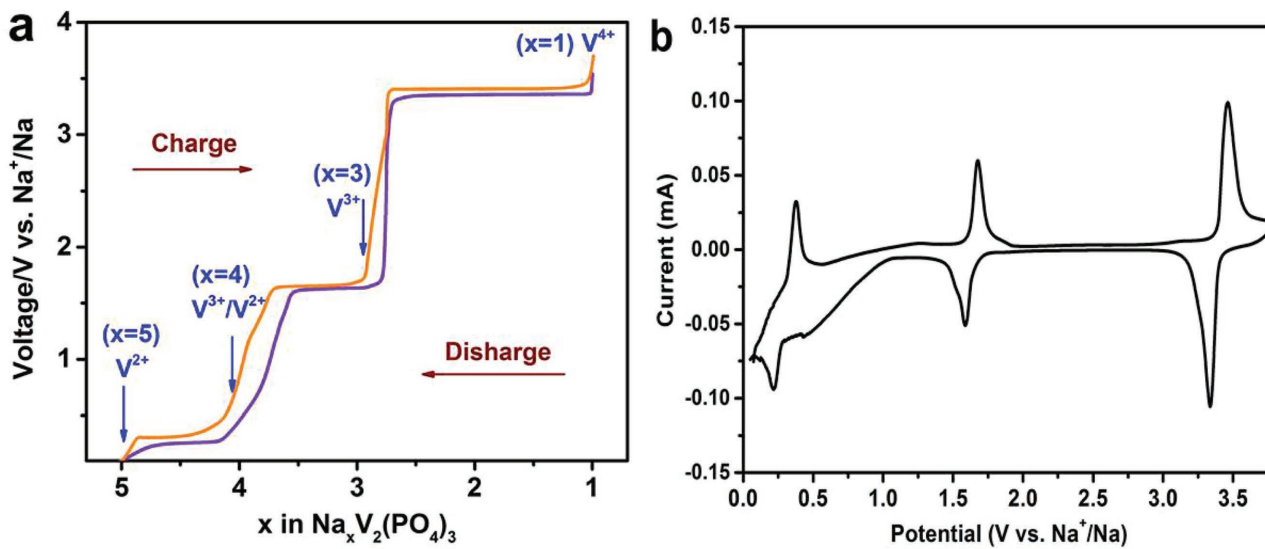


Figure 9. a,b) Electrochemical voltage–composition curves (a) and CV curve in the voltage range of 0.01–3.8 V vs Na⁺/Na (b) of Na₃V₂(PO₄)₃.

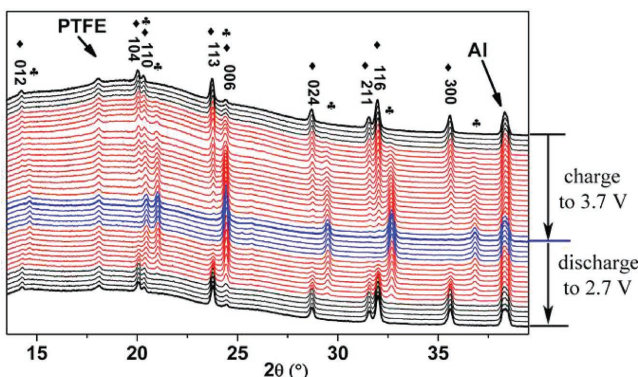


Figure 10. In situ XRD patterns of the $\text{Na}_3\text{V}_2(\text{PO}_4)_3/\text{Na}$ cell cycled between 3.7 and 2.7 V at a current rate of $\text{C}/10$: ♦ $\text{Na}_3\text{V}_2(\text{PO}_4)_3$, ♪ $\text{NaV}_2(\text{PO}_4)_3$. Reproduced with permission.^[64] Copyright 2013, Wiley-VCH.

with both electrodes having NVP encapsulated in a nanoporous carbon, which exhibited a power density exceeding 5.4 kW kg^{-1} at 11.7 A g^{-1} , a cycling life retention of 64.5% after 10 000 cycles at 1.17 A g^{-1} , and an energy density of 26 Wh kg^{-1} at 0.585 A g^{-1} (calculated based on the mass of both the cathode and the anode composites).^[74] Noguchi et al. developed an all-solid-state symmetric NIB based on NASICON-related compounds, where both electrodes were NVP, and the solid electrolyte was NASICON-structured $\text{Na}_3\text{Zr}_2\text{Si}_2\text{PO}_{12}$.^[75] The battery could deliver a capacity of 58 mA h g^{-1} . Lalère et al. prepared an

all-solid-state symmetric NIB, which operates at 1.8 V with 85% of the theoretical capacity attained at $200 \text{ }^\circ\text{C}$.^[76]

NVP has also been introduced to aqueous systems as well. The capacity of the NVP electrode reached 209 F g^{-1} at $8.5 \text{ }^\circ\text{C}$ (1 A g^{-1}) and the ion-diffusion coefficient was in the order of $\approx 10^{-10} \text{ cm}^2 \text{ s}^{-1}$.^[77] NVP is an important cathode material for NIBs, which shows a high operation potential, excellent cycling life, and ultrahigh rate performance. As an important class of NASICON electrode material, vanadium-based NASICON-type electrodes can be used as both the cathode and the anode because of their multiple redox couples. Their operation voltages are different in different materials (including different structures), where the relationship of operation voltage vs redox couples and alkyl ion number in $\text{A}_x\text{V}_2(\text{PO}_4)_3$ ($\text{A} = \text{Li}, \text{Na}, 0 \leq x \leq 5$) is summarized in Table 1.

2.3. Titanium-Based Materials

To our knowledge, there have been no reports on sulfates, molybdates, and tungstates of titanium-based NASICON-structured materials, which can be ascribed to the fact that Ti^{4+} is the thermodynamically stable valence state. Therefore, we focus on the phosphates.

Delmas and co-workers first reported the possible Li^+ - or Na^+ -ion-storage properties in $\text{LiTi}_2(\text{PO}_4)_3$ (LTP) and $\text{NaTi}_2(\text{PO}_4)_3$ (NTP), respectively, with both being rhombohedral.^[7b,78] LTP exhibits a high ionic conductivity of $\approx 10^{-6} \text{ S cm}^{-1}$, which can be

further enhanced by doping.^[79] The expected insertion product is $\text{A}_3\text{Ti}_2(\text{PO}_4)_3$ ($\text{A} = \text{Li}, \text{Na}$), corresponding to two-ion insertion. The insertion plateaus of Li^+ or Na^+ ions are located at 2.48 V vs Li^+/Li and 2.15 V vs Na^+/Na , respectively, corresponding to the same operation redox couple of $\text{Ti}^{4+}/\text{Ti}^{3+}$.^[7b,78] The difference of operation voltages reflects the potential gap between the Li^+/Li and Na^+/Na couples. Actually, $\text{Mg}_{0.5}\text{Ti}_2(\text{PO}_4)_3$ is also the host for Mg insertion. Makino et al. demonstrated Mg-ion insertion in $\text{Mg}_{0.5}\text{Ti}_2(\text{PO}_4)_3$, which shows 1.6 Mg-ion insertion with two plateaus located at -1.6 and -2.3 V vs Ag^+/Ag .^[9c]

The in situ XRD data reveal that Li-ion storage follows a typical two-phase reaction between $\text{LiTi}_2(\text{PO}_4)_3$ and $\text{Li}_3\text{Ti}_2(\text{PO}_4)_3$.^[80] With two Li^+ insertion, the $\text{R}\bar{3}\text{c}$ symmetry is no longer retained, where the stronger electrostatic repulsion between $[\text{Ti}_2(\text{PO}_4)_3]$ lanterns significantly increases the c/a ratio of the hexagonal unit cell. Aatiq et al. reported that three Li^+ ions reside on two similar tetrahedral sites, 18f, named M3' and M3'', in $\text{Li}_3\text{Ti}_2(\text{PO}_4)_3$, occupying $2/3$ and $1/3$ of the sites, respectively, while one Li^+ is located at 6b, named M1, in $\text{LiTi}_2(\text{PO}_4)_3$.^[81] In $\text{Na}_3\text{Ti}_2(\text{PO}_4)_3$ with $\text{R}\bar{3}\text{c}$ symmetry, one Na^+ fully occupies the 6b (M1) site, which is also occupied in NTP; another two Na^+ ions occupy the 18e (M2) sites with a $2/3$ occupancy ratio.^[82]

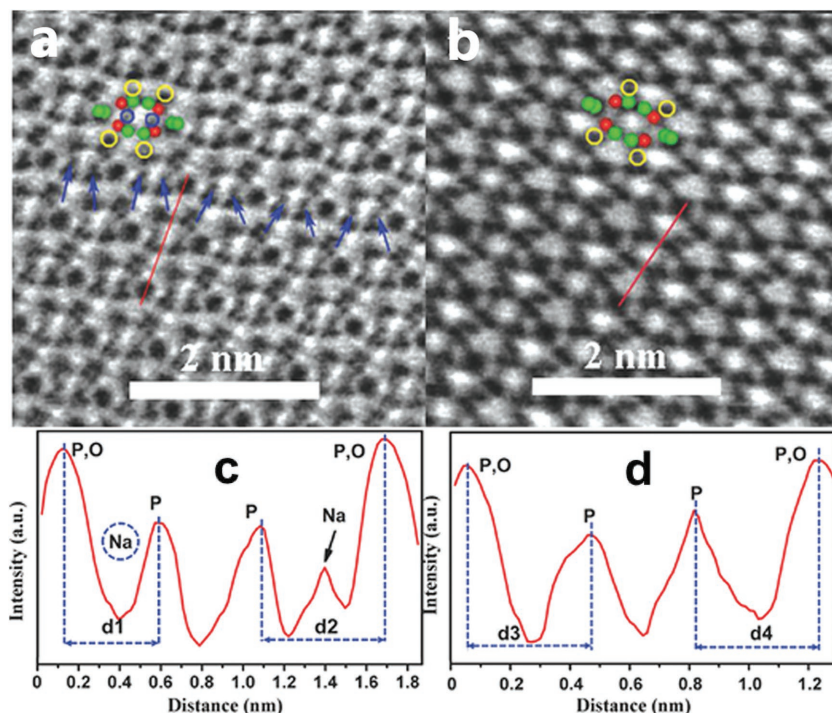


Figure 11. a,b) STEM ABF images of $\text{Na}_3\text{V}_2(\text{PO}_4)_3$ (a) and $\text{NaV}_2(\text{PO}_4)_3$ (b) along the^[67] projection (the blue and yellow circles are the Na atoms at the 6b and 18e sites respectively; the blue arrow indicates the Na atoms at the 18e site.). c,d) Line profiles along the ABF images of $\text{Na}_3\text{V}_2(\text{PO}_4)_3$ (c) and $\text{NaV}_2(\text{PO}_4)_3$ (d). In the ABF line profiles, the image contrast of the dark dots is inverted and displayed as peaks. Reproduced with permission.^[60] Copyright 2014, Wiley-VCH.

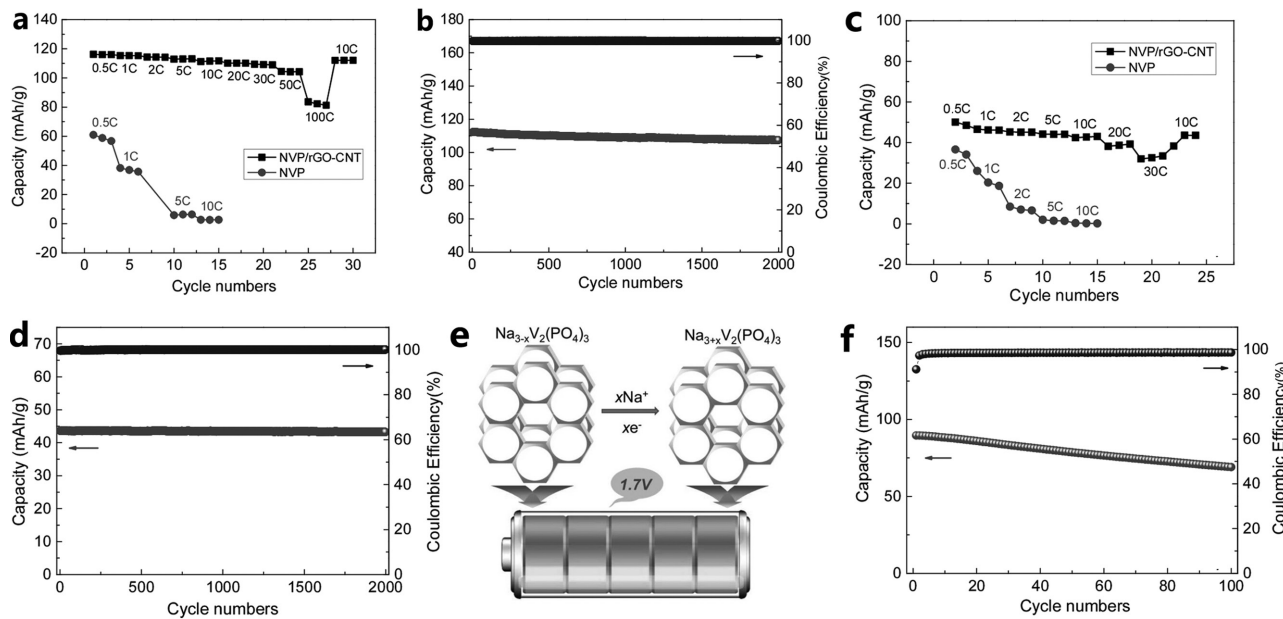


Figure 12. a,b) Rate capabilities of 3D porous NVP and interpenetrating 3D tricontinuous NVP:rGO–CNT as the cathode material (a) and as the anode material (b). c,d) Long cycling stability of interpenetrating 3D tricontinuous NVP: rGO–CNT and Coulombic efficiency as the cathode material (c) and as the anode material (d) for 2000 cycles at 10C. e) Schematic illustration of symmetric full sodium battery using interpenetrating 3D tricontinuous NVP:rGO–CNT as both the positive and the negative electrode. f) Typical charging/discharging profiles of such a symmetric full sodium battery for the first three cycles at 10C. Reproduced with permission.^[72] Copyright 2016, Wiley-VCH.

Aravindan et al. synthesized carbon-coated nano-LTP with a particle size of ≈ 80 nm, which showed a high capacity of 121 mA h g^{-1} with 83% capacity retention over 70 cycles.^[83] Huang et al. reported carbon-coated LTP nanoporous microplates that delivered a reversible capacity of 121 mA h g^{-1} and a capacity retention of 94.2% over 100 cycles in LIBs.^[84] Yang et al. obtained porous NTP nanocubes via a solvothermal method.^[85] The product presented a high capacity of 101 mA h g^{-1} and an excellent cycling stability with 75.5% capacity retention over 10 000 cycles at 10C.

In general, the operation voltages of the $\text{Ti}^{4+}/\text{Ti}^{3+}$ redox couple in LTP or NTP are considered to be too high to be used as anodes and too low to be employed as cathodes in non-aqueous LIBs or NIBs. Therefore, few studies have been carried out for NASICON-type LTP as an insertion host in non-aqueous electrolytes. In non-aqueous half-cells with a Li-metal counter electrode, LTP exhibits excellent rate performance, where its capacity reaches 103 mA h g^{-1} at 10C.^[86] Nevertheless, the

$\text{Ti}^{4+}/\text{Ti}^{3+}$ redox voltage in LTP or NTP is stable with respect to the lowest unoccupied molecular orbital (LUMO) of water as the anode in aqueous LIBs or NIBs.^[87] These aqueous metal-ion batteries can employ high-voltage cathodes,^[88] e.g., LiMn_2O_4 ^[89] and LiCoO_2 ,^[90] or other cathodes, e.g., $\text{Na}_{0.44}\text{MnO}_2$,^[91] $\text{Na}_{0.66}[\text{Mn}_{0.66}\text{Ti}_{0.34}]\text{O}_2$,^[92] $\text{Na}_2\text{CuFe}(\text{CN})_6$,^[93] and $\text{Na}_2\text{NiFe}(\text{CN})_6$.^[94] Luo et al. demonstrated carbon-coated LTP via the chemical vapor deposition (CVD) method.^[86] With LiMn_2O_4 as the cathode, LTP as the anode, and an aqueous electrolyte of 1 M Li_2SO_4 , a full-cell delivered a capacity of 40 mA h g^{-1} and an energy density of 60 Wh kg^{-1} based on the total mass of both the cathode and the anode materials. Furthermore, the cell exhibited a good cycling performance, maintaining $\approx 82\%$ of its initial reversible capacity after 200 cycles. Luo et al. further assembled LTP/ $\text{Li}_2\text{SO}_4/\text{LiFePO}_4$ aqueous LIBs, which showed superior cycling capability after eliminating O_2 .^[95] The capacity retention was over 90% after 1000 cycles at 6C and 85% after 50 cycles even at a very low current rate of C/8. Sun et al. synthesized LTP@nitrogen-rich doped carbon composites, and LTP composite/ $\text{Li}_2\text{SO}_4/\text{LiMn}_2\text{O}_4$ aqueous LIBs were assembled. The full-cell demonstrated a superior rate capability of 103 mA h g^{-1} at 10C and an outstanding cycling stability with capacity retention of 90.4% over 400 cycles at a current rate of 150 mA g^{-1} (based on the LTP mass).^[96]

Park et al. first reported an NTP electrode for aqueous NIBs and assembled NTP/Zn aqueous NIBs, which delivered a high capacity of 123 mA h g^{-1} , good cycling stability, and superior rate performance.^[97] Li et al. demonstrated NTP/ $\text{Na}_{0.44}\text{MnO}_2$ aqueous NIBs that exhibited ultrafast rate capability ($>100\text{C}$) and superior cycling stability (>1500 cycles).^[98] Wu et al. synthesized graphite-coated NTP, and assembled NTP/ $\text{Na}_{0.44}\text{MnO}_2$

Table 1. The relationship of operation voltages vs redox couples and x in $\text{A}_x\text{V}_2(\text{PO}_4)_3$.

Redox couple	x in material	m-LVP [V vs Li^+/Li]	r-LVP [V vs Li^+/Li]	NVP [V vs Na^+/Na]
V^{5+}/V^4	0	4.6	—	—
$\text{V}^{4+}/\text{V}^{3+}$	1	4.1	3.7	3.4
	2	3.7 and 3.6	3.7	3.4
$\text{V}^{3+}/\text{V}^{2+}$	4	1.9 and 1.8	1.75	1.75
	5	1.7 and 1.6	1.75	1.75

aqueous cells, which showed a high capacity of 130 mA g⁻¹ at 0.1C and relatively good cyclability at 1C with 86% capacity retention over 100 cycles.^[99] Wang et al. investigated the electrochemical performance of NTP/Na_{0.44}[Mn_{0.44}Ti_{0.56}]O₂ and NTP/Na_{0.66}[Mn_{0.66}Ti_{0.34}]O₂ aqueous batteries (Figure 13), which showed similar operation voltages, but a higher capacity in an NTP/Na_{0.66}[Mn_{0.66}Ti_{0.34}]O₂ aqueous battery. An NTP/Na_{0.66}[Mn_{0.66}Ti_{0.34}]O₂ cell also exhibited excellent rate and cycling performance.^[92] Wu et al. assembled NTP/Na₂CuFe(CN)₆ cells that could deliver a high average voltage of 1.4 V, an energy density of 48 Wh kg⁻¹, and an excellent high-rate cycling stability with approximately 90% capacity retention over 1000 cycles at 10C (Figure 14a,b).^[93] Wu et al. also demonstrated that the NTP/Na₂NiFe(CN)₆ aqueous cell provided an average output voltage of 1.7 V and an energy density of 42.5 Wh kg⁻¹, and could retain 88% of its initial capacity over 250 cycles at 5C (Figure 14c,d).^[94]

Besides aqueous batteries, ATi₂(PO₄)₃ (A = Li, Na) has also been introduced into solid-state batteries. NTP/Na cells with NaTFSI/PEO [sodium bis(trifluoromethanesulfonyl)-imide/poly(ethylene oxide)] as an electrolyte showed a stable capacity of ≈80 mA h g⁻¹ over 100 cycles at 0.5C and 65 °C.^[100] Most titanium-based NASICON-type materials operate on Ti⁴⁺/Ti³⁺.^[101] However, Senguttuvan et al. introduced Na₃Ti₂(PO₄)₃ symmetric full-cell NIBs, which delivered an operation voltage of 1.7 V.^[102] Na₃Ti₂(PO₄)₃ with a triclinic structure not only can be oxidized to NaTi₂(PO₄)₃ (rhombohedral structure), but also

can be reduced to Na₄Ti₂(PO₄)₃ (rhombohedral structure), corresponding to 2.1 and 0.4 V vs Na⁺/Na, respectively.

ATi₂(PO₄)₃ represents a very promising group of anodes in aqueous batteries due to its stable structure, high capacity, and suitable voltage. Furthermore, ATi₂(PO₄)₃ exhibits high ionic conductivity, especially after doping; we will review these materials as electrolytes in Section 3.

2.4. Multi-Transition-Metal-Based Materials

Nanjundaswamy et al. synthesized monoclinic FeTi(SO₄)₃ and Li₃FeV(PO₄)₃, where the redox couples include Fe³⁺/Fe²⁺(I) at 3.6 V, Fe³⁺/Fe²⁺(II) at 3.2 V, Ti³⁺/Ti²⁺ at 1.7 V, and Fe³⁺/Fe²⁺ at 2.8 V, V⁴⁺/V³⁺ at 3.8 V, V³⁺/V²⁺ at 1.75 V vs Li⁺/Li, respectively.^[9a] Padhi et al. also demonstrated a series of multi-transition-metal NASICON materials, such as Li₂NaFeV(PO₄)₃, Li₂Na₂FeV(PO₄)₃, Li₂FeTi(PO₄)₃, TiNb(PO₄)₃, and LiFeNb(PO₄)₃.^[103] The positions of the redox couples were determined with respect to the Fermi energy of lithium, as shown in Figure 15: V⁴⁺/V³⁺ at 3.8 V, Fe³⁺/Fe²⁺ at 2.8 V, Ti⁴⁺/Ti³⁺ at 2.5 V, Nb⁵⁺/Nb⁴⁺ at 2.2 V, Nb⁴⁺/Nb³⁺ at 1.8 V, and V³⁺/V²⁺ at 1.7 V vs Li⁺/Li. Patoux et al. reported the structure and electrochemical performance of Li_{1.6}Na_{0.4}TiM(PO₄)₃ (M = Fe, Cr), which is of a rhombohedral NASICON structure and shows stable cyclability.^[104] Two Li⁺ ions can be inserted into Li_{1.6}Na_{0.4}TiFe(PO₄)₃, while only one Li⁺ ion can be inserted into Li_{1.6}Na_{0.4}TiCr(PO₄)₃ due to

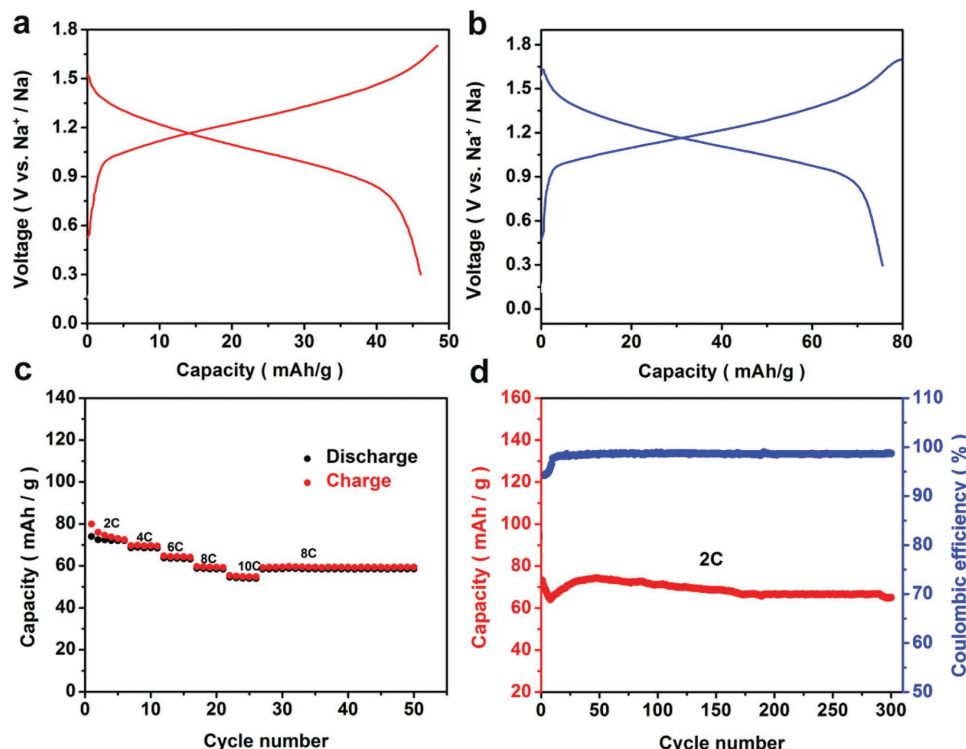


Figure 13. a,b) The typical charge/discharge curves in the voltage range of 0.3–1.7 V for NTP/Na_{0.44}[Mn_{0.44}Ti_{0.56}]O₂ (a) and NTP/Na_{0.66}[Mn_{0.66}Ti_{0.34}]O₂ (b) full-cells at a current rate of 2C. c) Rate performance of an NTP/Na_{0.66}[Mn_{0.66}Ti_{0.34}]O₂ full-cell cycled in the voltage range of 0.3–1.7 V at various current rates. d) Cycling performance of an NTP/Na_{0.66}[Mn_{0.66}Ti_{0.34}]O₂ full-cell at a current rate of 2C. Reproduced with permission.^[92] Copyright 2015, Wiley-VCH.

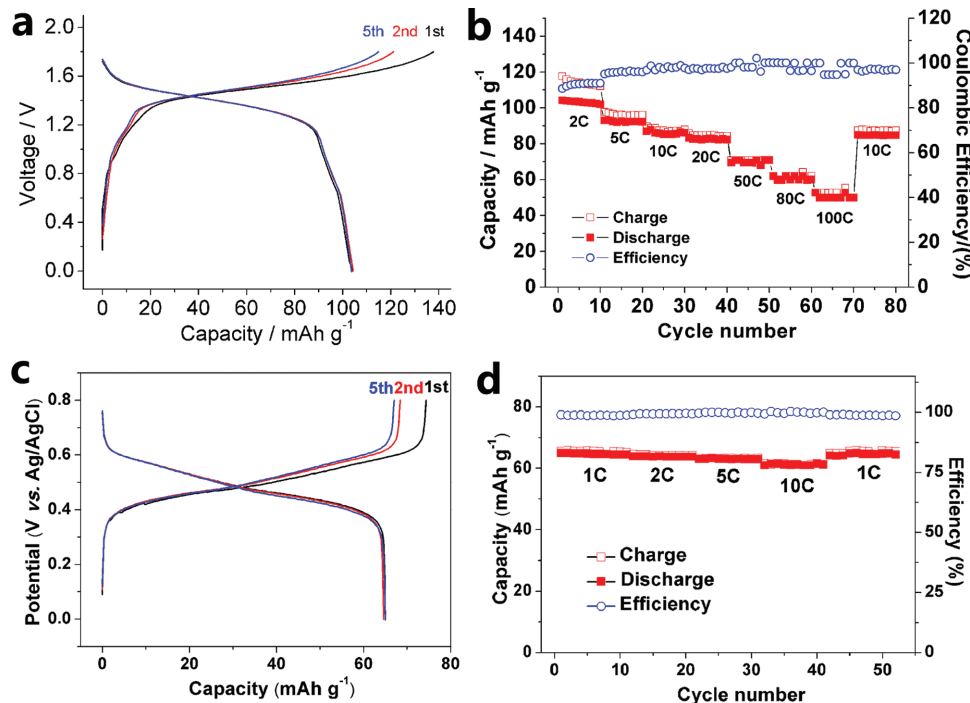


Figure 14. Electrochemical performance of the NTP/Na₂CuFe(CN)₆ full-cells: a) charge/discharge curves at a current density of 2C; the capacity was calculated based on the mass of the anode; b) rate performance from 2C to 100C; c) discharge curves at different rates 2C to 100C; d) long-term cycling performance of the full-cell at 10C rates. a,b) Reproduced with permission.^[93] Copyright 2014, Wiley-VCH. c,d) Reproduced with permission.^[94] Copyright 2013, Elsevier.

the inactive Cr³⁺. In situ XRD data of Li⁺-ion insertion into Li_{1.6}Na_{0.4}TiCr(PO₄)₃ indicate a solid-solution reaction, where the diffraction peaks continuously shift to lower angles. The

Li-storage mechanism with solid-solution reaction was also confirmed by potentiostatic intermittent titration technique (PITT) results.^[104]

In the early 1990s, Quarton's group investigated a series of mixed NASICON-type materials: Na_xMM'(PO₄)₃ (M = Fe, Ti, Nb, Sc), such as Na_xTiNb(PO₄)₃, Na_{1+x}FeNb(PO₄)₃, and Na_{2+x}FeTi(PO₄)₃.^[105] It is interesting to note that the positions of the redox couples are mostly independent, due to the absence of direct connectivity between the two (MM')O₆ octahedra. For example, the potential of the Ti⁴⁺/Ti³⁺ redox couple in Na_xTiNb(PO₄)₃ and Na_{2+x}FeTi(PO₄)₃ is similar to that in NaTi₂(PO₄)₃.^[106] It was also confirmed by Patoux et al., who synthesized Na_{2+x}TiM(PO₄)₃ (M = Fe, Cr)^[104] and demonstrated that Na⁺-ion insertion into Na₂TiFe(PO₄)₃ and Na₂TiCr(PO₄)₃ proceeds as single-phase reactions.^[104] However, Tillement et al. showed a nearly flat plateau on discharge of Na₂TiFe(PO₄)₃, which indicates a two-phase reaction between Na₂TiFe(PO₄)₃ and Na_{2.5}TiFe(PO₄)₃.^[105b]

A large number of NASICON-type electrode materials have been investigated, where the operation voltage can be tuned by different transition-metal redox couples and/or polyanion groups. Meanwhile, the structures determine the electrochemical performance, despite the same composition, such as r-LVP and m-LVP in Section 2.2. The previous section shows a plateau corresponding to the extraction of two Li⁺ ions from r-LVP, whereas the m-LVP shows four plateaus in the charge curve corresponding to the extraction of 3 Li⁺ ions. All three Li⁺ ions that occupy the different sites are mobile, resulting in a high capacity and several plateaus. The r-LVP is obtained from NVP by ion exchange, which shows the same structure

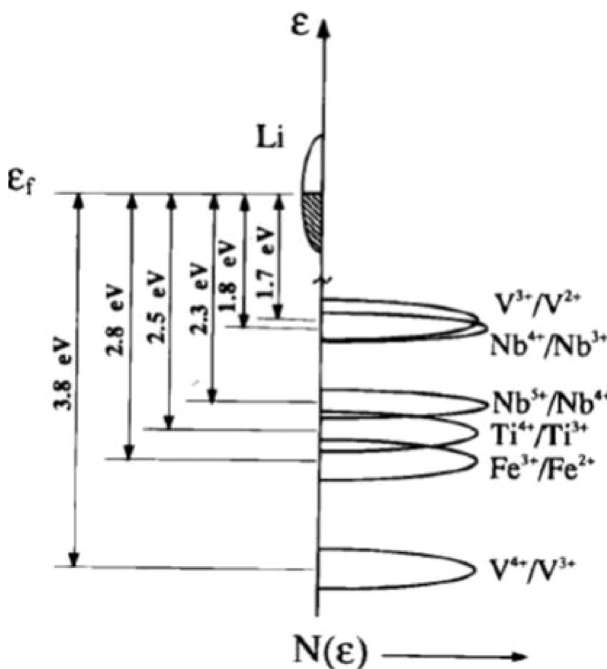


Figure 15. Relative energies of different redox couples. Reproduced with permission.^[103] Copyright 1997, The Electrochemical Society.

and the same charge/discharge curves for the cathode (except for the voltage difference between Li^+/Li and Na^+/Na). In NVP, three Na^+ ions occupy two different sites (one in the 6b sites and two in the 18e sites), where only the two Na^+ ions occupying the 18e sites are mobile, leading to moderate capacity and a single plateau. Furthermore, the electrochemical performance can also be greatly improved by doping, shortening the ion-diffusion pathway, and by carbon coating. NASICON-type materials are an important class of electrodes for LIBs and NIBs.

3. Solid Electrolytes

3.1. NASICON-Type Na^+ -Ion Conductors

Since the pioneer work by Hong, Goodenough, and Kafalas in 1976,^[6] the family of NASICON compounds has gained much attention as solid electrolytes. The solid solution $\text{Na}_{1+x}\text{Zr}_2\text{P}_{3-x}\text{Si}_x\text{O}_{12}$ ($0 \leq x \leq 3$) was prepared, and their structure and ionic conductivity were investigated.^[6b] The structure maintains a space group of $\text{R}\bar{3}\text{c}$ (rhombohedra) for all compositions except for those in the range of $1.8 \leq x \leq 2.2$, which show a monoclinic structure ($\text{C}2/\text{c}$ group). The monoclinic $\text{Na}_{1+x}\text{Zr}_2\text{P}_{3-x}\text{Si}_x\text{O}_{12}$ ($1.8 \leq x \leq 2.2$), particularly when $x = 2$, presents the highest ionic conductivity, which can reach $2.0 \times 10^{-1} \text{ S cm}^{-1}$ at 300°C and $6.7 \times 10^{-4} \text{ S cm}^{-1}$ at room temperature. The rhombohedral $\text{Na}_{1+x}\text{Zr}_2\text{P}_{3-x}\text{Si}_x\text{O}_{12}$ shows lower ionic conductivity, especially in $\text{NaZr}_2\text{P}_3\text{O}_{12}$. The conduction pathways of sodium ions ($\text{Na}(1) \rightarrow \text{Na}(2) \rightarrow \text{Na}(1)$ sites) are of a zigzag geometry (see Figure 16^[107]).^[108] Zhang et al. synthesized $\text{NaZr}_2\text{P}_3\text{O}_{12}$ by a sol-gel method, which showed a high ionic conductivity ($5.4 \times 10^{-4} \text{ S cm}^{-1}$ at room temperature).^[109] A noble metal was also introduced to the NASICON solid electrolyte. $\text{Na}_{1+x}\text{Hf}_2\text{Si}_x\text{P}_{3-x}\text{O}_{12}$ exhibits very high ionic conductivities, where the values of $\text{Na}_{3.2}\text{Hf}_2\text{Si}_{2.2}\text{P}_{0.8}\text{O}_{12}$ are $2.3 \times 10^{-3} \text{ S cm}^{-1}$ at room temperature and 0.224 S cm^{-1} at

300°C .^[110] However, the cost is much higher compared with $\text{Na}_3\text{Zr}_2\text{Si}_2\text{PO}_{12}$, due to the use of hafnium. Tillement et al. synthesized $\text{Na}_{2+x+y}\text{Zr}_{1-y}\text{Fe}_x\text{Fe}_{1-x+y}(\text{PO}_4)_3$ ($y = 0, 0 \leq x \leq 1; x + y = 1, 0 \leq y \leq 0.5$), where Fe is of different oxidation states. The highest ionic conductivity in these materials is $4 \times 10^{-3} \text{ S cm}^{-1}$ at 300°C .^[105a] Asai et al. investigated $\text{Na}_{1+4x}\text{M}_x\text{Fe}_{2x}\text{Zr}_{2-3x}(\text{PO}_4)_3$ ($\text{M} = \text{Fe}, \text{Co}, \text{and Ni}$), where the ionic conductivities were close to $7 \times 10^{-3} \text{ S cm}^{-1}$ at 300°C .^[111] Bohnke et al. measured the ionic conductivities of $\text{Na}_3\text{Zr}_{2-x/4}\text{Si}_{2-x}\text{P}_{1+x}\text{O}_{12}$ ($0 < x < 2$).^[108a] The bulk ionic conductivity decreased slightly from $6 \times 10^{-4} \text{ S cm}^{-1}$ for the Zr non-deficient NASICON ($x = 0$) to $6 \times 10^{-5} \text{ S cm}^{-1}$ for the most-Zr-deficient material ($x = 1.667$).

$\text{Na}_3\text{Zr}_2\text{Si}_2\text{PO}_{12}$ has a very high conductivity and low cost, and has been commercialized in CO_2 sensors.^[108a] Gordon et al. fabricated a room-temperature Na–S battery with this material as a solid-state electrolyte, which delivered a capacity of 350 mA h g^{-1} (based on the sulfur mass).^[67] Hashimoto et al. assembled aqueous and non-aqueous $\text{Na}-\text{O}_2$ batteries with $\text{Na}_3\text{Zr}_2\text{Si}_2\text{PO}_{12}$ as the electrolyte and separator at room temperature.^[112] The aqueous battery showed low polarization ($\approx 0.6 \text{ V}$) and a high round-trip efficiency. Hayashi et al. also fabricated aqueous $\text{Na}-\text{O}_2$ batteries, which exhibited a high capacity of 600 mA h g^{-1} and a high energy density.^[113] Kim et al. designed a pouch-type flexible solid-state full-cell with hard carbon as the anode, NaFePO_4 as the cathode, and a $\text{Na}_3\text{Zr}_2\text{Si}_2\text{PO}_{12}$ -based composite as the hybrid solid electrolyte (HSE).^[110] The HSE exhibited a high ionic conductivity of $3.6 \times 10^{-4} \text{ S cm}^{-1}$ at room temperature. The battery delivered a high capacity of 120 mA h g^{-1} and an average voltage of 2.6 V (Figure 17a). It showed very stable cycling capability and high Coulombic efficiency (Figure 17b). However, the NASICON materials are not stable in contact with molten sodium.^[114] Schmid et al. confirmed that $\text{Na}_{1+x}\text{Zr}_2\text{P}_{3-x}\text{Si}_x\text{O}_{12}$ with $x = 2$ or 2.2 is chemically attacked, rendering it unstable for high-temperature Na–S batteries.^[114]

3.2. NASICON-Type Li^+ -Ion Conductors

With the rapid development of LIBs, NASICON-type Li-ion conductors have been of great interest. $\text{Li}_{1+x}\text{M}_{2-x}\text{M}'_x(\text{PO}_4)_3$ where $\text{M} = \text{Ti}, \text{Ge}$, and Hf ; $\text{M}' = \text{In}^{3+}$,^[115] Sc^{3+} ,^[79a,116] Ga^{3+} ,^[116a,117] Cr^{3+} ,^[118] Al^{3+} ,^[115c,118b,119] and Fe^{3+} ,^[120] have been investigated, where the Al-doped ceramics show excellent ionic conductivities. The nominal composition $\text{Li}_{1.3}\text{Al}_{0.3}\text{Ti}_{1.7}(\text{PO}_4)_3$ was reported by Arbi et al., which had high Li^+ ionic conductivities: $7 \times 10^{-4} \text{ S cm}^{-1}$ at room temperature and 0.1 S cm^{-1} at 300°C . In the $\text{Li}_{1+x}\text{Ti}_{2-x}\text{Al}_x(\text{PO}_4)_3$ system, which has been commercialized by OHARA Inc., smaller Al^{3+} substitutes the Ti^{4+} cations, which reduces the unit-cell dimensions of the NASICON frameworks and enhances the ionic conductivity by 3 orders of magnitude.^[119b] Kotobuki et al. synthesized $\text{Li}_{1.5}\text{Al}_{0.5}\text{Ti}_{1.5}(\text{PO}_4)_3$ by a co-precipitation method, where

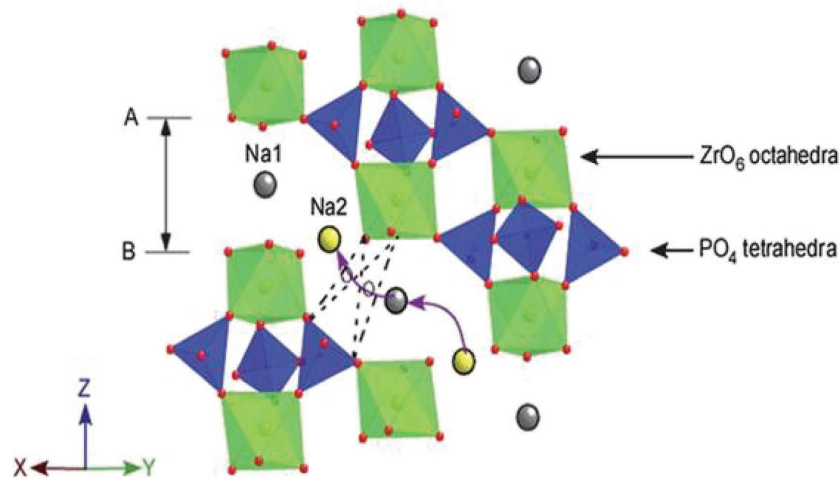


Figure 16. NASICON structure in rhombohedral symmetry, showing ZrO_6 and $(\text{Si}, \text{P})\text{O}_4$ polyhedra. The dark-shaded circles represent the $\text{Na}(1)$ positions, the light-shaded circles represent the $\text{Na}(2)$ positions, and the curved arrow represents the conduction path of Na^+ ions. Reproduced with permission.^[107] Copyright 2013, Royal Society of Chemistry.

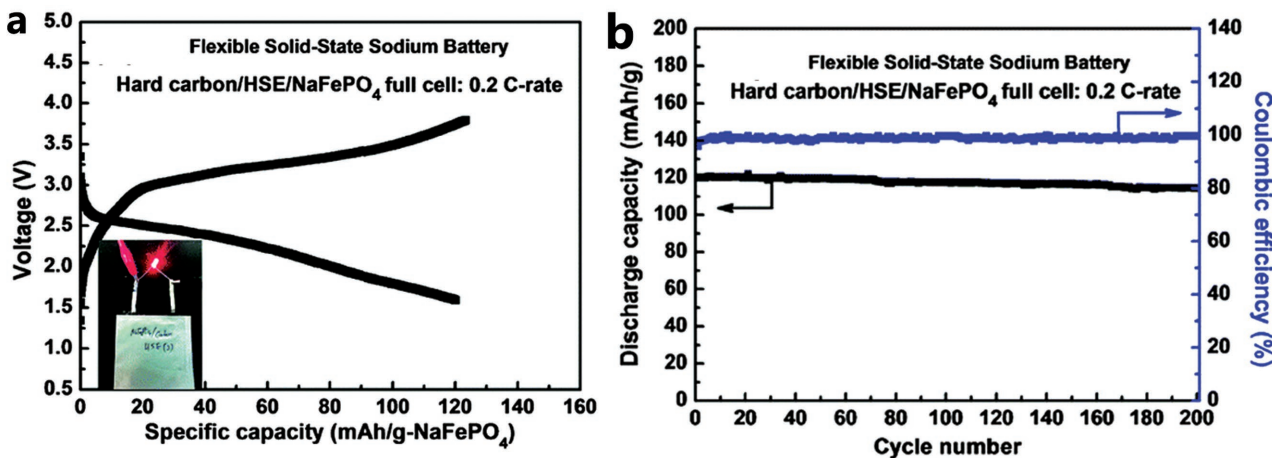


Figure 17. a) Initial charge/discharge curve and b) cycle performances and Coulombic efficiency of a flexible full-cell for a hard-carbon/HSE/NaFePO₄ battery, which was tested in a pouch-type full cell at room temperature.

Li_{1.5}Al_{0.5}Ti_{1.5}(PO₄)₃ exhibited a high room-temperature ionic conductivity of 1.4×10^{-3} S cm⁻¹.^[121] Recently Arbi et al. compared Li_{1+x}Al_xTi_{2-x}(PO₄)₃ and Li_{1+x}Al_xGe_{2-x}(PO₄)₃, where Li_{1+x}Al_xTi_{2-x}(PO₄)₃ showed a higher ionic conductivity of 3.4×10^{-3} S cm⁻¹ at room temperature when x was 0.2 or 0.4.^[122] Solid electrolytes are essential to fabricate practical solid-state devices, including LIBs^[123] and Li-air batteries, which can be safer.

Birke et al. fabricated a solid-state Li₄Ti₅O₁₂/Li_{1.3}Al_{0.3}Ti_{1.7}(PO₄)₃/LiMn₂O₄ cell, which exhibited a charge/discharge plateau at \approx 2.5 V.^[124] Inda et al. also reported a solid-state Li₄Ti₅O₁₂/Li_{1+x+y}Al_xTi_{2-x}Si_yP_{3-y}O₁₂/LiCoO₂ cell that showed a plateau at \approx 2.4 V with a high capacity of 150 mA h g⁻¹.^[125] There is a high interfacial resistance between a solid electrolyte and the electrodes. In order to overcome this problem, a buffer layer of a polymer electrolyte, e.g., poly(ethylene oxide) (PEO):lithium electrolyte salts, e.g., Li(CF₃SO₂)₂N, or PEO:Li₂O, (named a polymer electrolyte (PE)), is often incorporated between the electrodes and a solid electrolyte, which can effectively reduce the charge-transfer resistance.^[126] As is known, Ti⁴⁺ is not cathodically stable in NASICON-type materials. The buffer layer is also used to avoid the direct contact of Li_{1+x+y}Al_xTi_{2-x}Si_yP_{3-y}O₁₂ (LATP) with a Li-metal anode to avoid the reduction of Ti⁴⁺.^[126] Xie et al. reported a Li/PE/LATP/LiCoO₂ cell with a high

operation voltage of 3.8 V.^[126a] They also investigated the lithium-storage properties of a series of cathodes in solid-state Li/PE/LATP/cathode cells.^[127]

Kumar et al. assembled a Li-O₂ battery with a PE/Li_{1+x}Al_xGe_{2-x}(PO₄)₃ (LAGP) solid-state electrolyte, where the capacity was found to be dependent on the operation temperature.^[128] The Li-O₂ cell exhibited a high energy density of 3500 Wh kg⁻¹. Kitaura and Zhou fabricated a Li/PE/LATP/CNT@LATP-O₂ battery, which exhibited a high capacity of 400 mA h g⁻¹ with an average discharge voltage of 2.9 V.^[129] They identified a large cell resistance, which limits its rate performance, and which mainly comes from the interfacial resistance between the Li metal and the polymer electrolyte. To overcome this problem, they adhered lithium metal onto one side of an LAGP pellet by a thermal melting method.^[129] Such a Li/LAGP/LAGP@CNT-air battery was built and presented excellent electrochemical performance (Figure 18).

LTAP has been commonly utilized as a separator for hybrid battery systems with both non-aqueous and aqueous electrolyte compartments.^[130] Li et al. built a Li/organic electrolyte/LTAP/aqueous electrolyte/Ni(OH)₂ battery, which exhibited 250 mA h g⁻¹ with an average voltage of 3.5 V.^[131] Zhang and Zhou demonstrated a Li/EC-based electrolyte/LTAP/CNT gel battery, which delivered an ultrahigh reversible capacity of

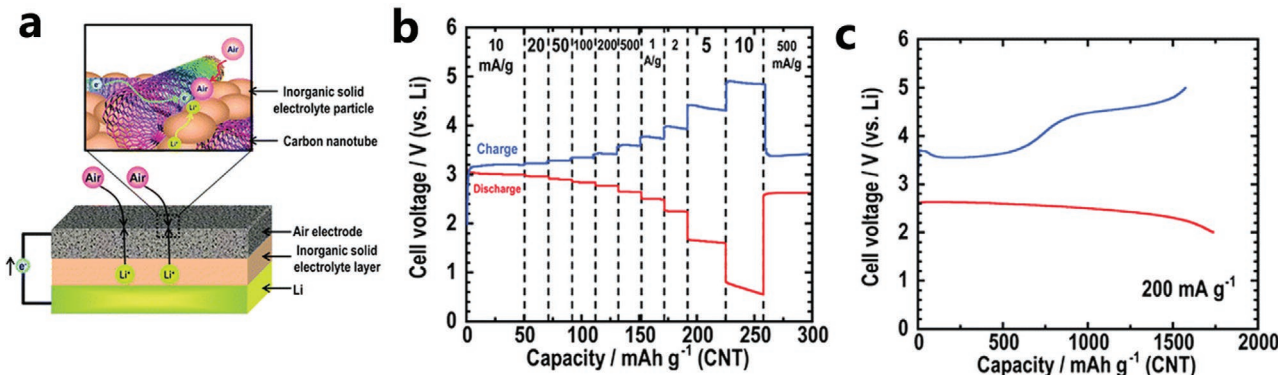


Figure 18. a) Schematic diagram of a solid-state Li/LAGP/LAGP@CNT-air battery. b,c) Rate performance (b) and first charge/discharge curves (c) of the solid-state battery. Reproduced with permission.^[129] Copyright 2012, Royal Society of Chemistry.

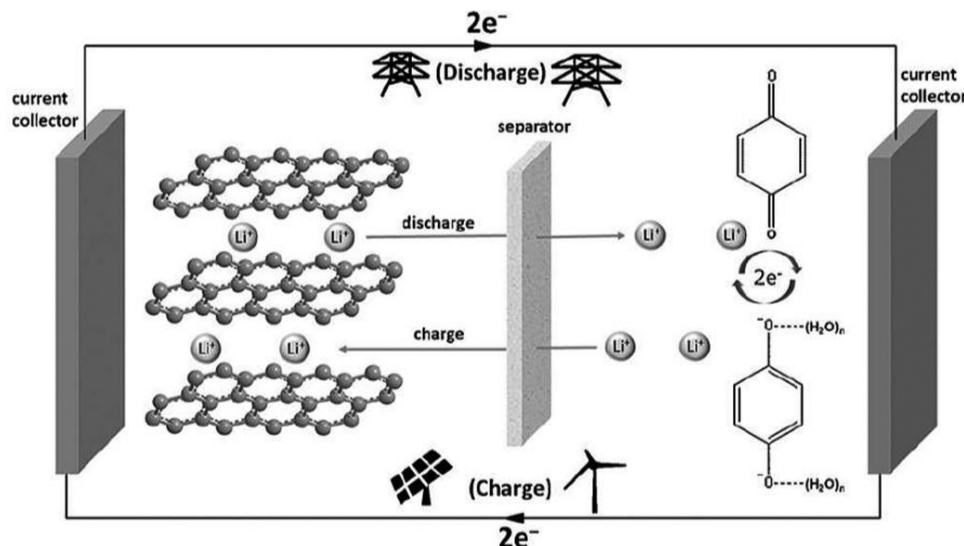


Figure 19. Working principle of the designed liquid battery with H₂BQ aqueous solution as the catholyte and graphite in organic electrolyte as the anode. Reproduced with permission.^[133] Copyright 2016, Wiley-VCH.

$\approx 55\,000 \text{ mA h g}^{-1}$ (based on the catalyst carbon mass).^[132] Ding and Yu demonstrated a graphite/organic electrolyte/LTAP/hydroquinone aqueous battery (Figure 19), which showed a capacity of 500 mA h g^{-1} with a potential of 3.5 V.^[133] Li et al. designed a Li–O₂ battery with a hybrid electrolyte comprising organic electrolyte/LTAP/aqueous electrolyte and NiCo₂O₄ and N-doped mesoporous carbon as the cathode (Figure 20), where the NiCo₂O₄ worked as the oxygen-evolution reaction (OER) catalyst and the N-doped mesoporous carbon served as the oxygen-reduction reaction (ORR) catalyst.^[134] This cell presented an excellent cycle life.

4. Conclusion and Prospects

NASICON type materials are considered as a class of 3D framework compounds possessing a stable structure and high ionic conductivity, leading to their wide applications, including energy-storage, membranes, fuel cells and gas sensors. This review presents the state of the art of NASICON as Li-ion or Na-ion storage materials, and solid-state electrolytes, along with their applications. Usually, the operation potentials show the following trend: V⁵⁺/V⁴⁺ > V⁴⁺/V³⁺ > Fe³⁺/Fe²⁺ > Ti⁴⁺/Ti³⁺ > Nb⁵⁺/Nb⁴⁺ > Nb⁴⁺/Nb³⁺ > V³⁺/V²⁺ > Ti³⁺/Ti²⁺. On the other

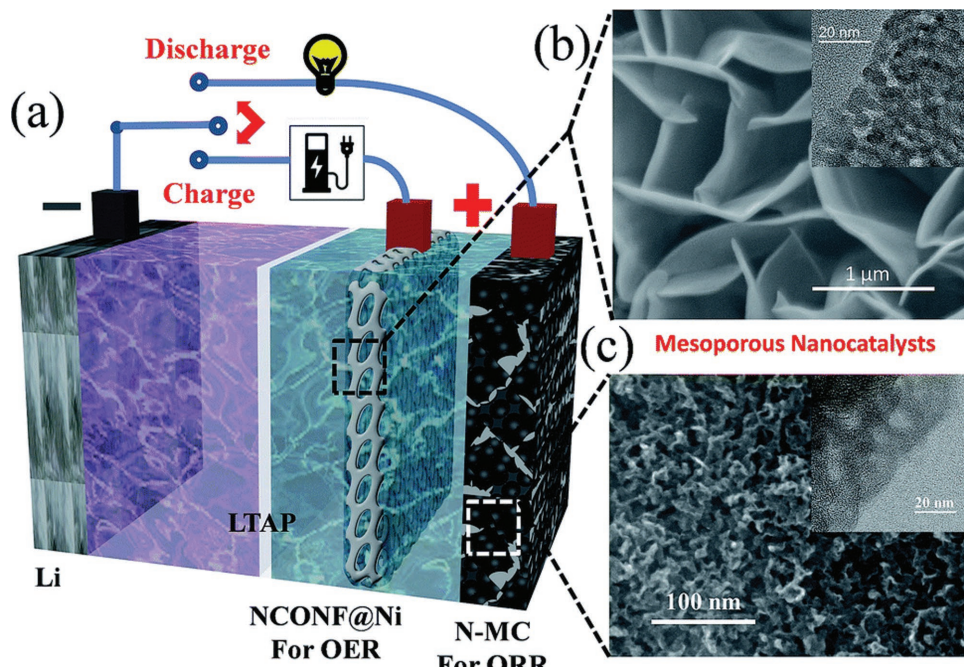


Figure 20. Schematic representation of the hybrid Li–air cell with mesoporous nanocatalysts. Reproduced with permission.^[134] Copyright 2014, Royal Society of Chemistry.

hand, polyanions also lead to different potentials, which is called the inductive effect. It is known that the weak M–O bands (the NASICON structure has the formula of $A_xMM'(XO_4)_3$) can raise the operation voltage of the same redox couple. Therefore, NASICON-type materials with high electronegative polyanions will present high operation potentials due to their stronger electron-withdrawing capability. The electrochemical performance of NASICON can be greatly improved by carbon coating, decreasing the particle size and doping. The structural evolution has also been investigated to understand the ion-storage mechanisms.

To avoid the risk of thermal runaway, solid-state batteries have been proposed as a fundamental solution. Solid-state batteries face great challenges, especially, the low intrinsic ionic conductivity of solid electrolytes and large interfacial resistance between electrodes and the electrolyte. To overcome the former problem, new solid electrolyte materials with high intrinsic ionic conductivity should be developed. NASICON-type electrolytes can supply a choice. For Li-based solid-state electrolytes, LATP shows high ionic conductivity and low cost, while LAGP is also widely studied due to its better stability than LATP. Many types of solid-state batteries and hybrid batteries have been fabricated, exhibiting superior electrochemical performance and expanding the family of battery systems. Concerning the latter problem, NASICON-type materials can be used for the cathode, anode, and electrolyte. Therefore, all-NASICON solid-state batteries can be fabricated. It can form an electrolyte buffer layer of a solid-solution or composite between NASICON electrodes and electrolyte, which can build fast ionic channels, leading to a low interfacial resistance.

Acknowledgements

W.C. gratefully acknowledges the support from NSFC (No. 51072152, 50672071, 50172036, China). X.J. thanks the financial support from the National Science Foundation of the United States, Award Number: 1507391. Y.-S.H. thanks the financial support from the National Key Technologies R&D Program (Grant No. 2016YFB0901504) and the NSFC (No. 51222210, China).

Received: April 11, 2016

Revised: November 21, 2016

Published online: February 21, 2017

- [1] a) J. Baxter, Z. Bian, G. Chen, D. Danielson, M. S. Dresselhaus, A. G. Fedorov, T. S. Fisher, C. W. Jones, E. Maginn, U. Kortshagen, *Energy Environ. Sci.* **2009**, *2*, 559; b) B. Dunn, H. Kamath, J.-M. Tarascon, *Science* **2011**, *334*, 928; c) M. Armand, J.-M. Tarascon, *Nature* **2008**, *451*, 652.
- [2] a) X. L. Wu, L. Y. Jiang, F. F. Cao, Y. G. Guo, L. J. Wan, *Adv. Mater.* **2009**, *21*, 2710; b) B. Scrosati, J. Hassoun, Y.-K. Sun, *Energy Environ. Sci.* **2011**, *4*, 3287.
- [3] a) K. Mizushima, P. Jones, P. Wiseman, J. Goodenough, *Mater. Res. Bull.* **1980**, *15*, 783; b) N. Yabuuchi, M. Takeuchi, M. Nakayama, H. Shiiba, M. Ogawa, K. Nakayama, T. Ohta, D. Endo, T. Ozaki, T. Inamasu, *PNAS* **2015**, *112*, 7650.
- [4] a) Z. Gong, Y. Yang, *Energy Environ. Sci.* **2011**, *4*, 3223; b) D.-W. Han, S.-J. Lim, Y.-I. Kim, S. H. Kang, Y. C. Lee, Y.-M. Kang, *Chem. Mater.* **2014**, *26*, 3644.

- [5] a) C. Masquelier, L. Croguennec, *Chem. Rev.* **2013**, *113*, 6552; b) L. Wang, J. Bai, P. Gao, X. Wang, J. P. Looney, F. Wang, *Chem. Mater.* **2015**, *27*, 5712; c) N. Membreño, K. Park, J. B. Goodenough, K. J. Stevenson, *Chem. Mater.* **2015**, *27*, 3332.
- [6] a) J. Goodenough, H.-P. Hong, J. Kafalas, *Mater. Res. Bull.* **1976**, *11*, 203; b) H.-P. Hong, *Mater. Res. Bull.* **1976**, *11*, 173.
- [7] a) C. Delmas, A. Nadiri, J. Soubeyroux, *Solid State Ionics* **1988**, *28*, 419; b) C. Delmas, F. Cherkaoui, A. Nadiri, P. Hagenmuller, *Mater. Res. Bull.* **1987**, *22*, 631.
- [8] a) X. Rui, Q. Yan, M. Skyllas-Kazacos, T. M. Lim, *J. Power Sources* **2014**, *258*, 19; b) Pan, Y.-S. Hu, L. Chen, *Energy Environ. Sci.* **2013**, *6*, 2338; c) H. Li, Z. Wang, L. Chen, X. Huang, *Adv. Mater.* **2009**, *21*, 4593; d) A. Robertson, A. West, A. Ritchie, *Solid State Ionics* **1997**, *104*, 1; e) N. Anantharamulu, K. K. Rao, G. Rambabu, B. V. Kumar, V. Radha, M. Vithal, *J. Mater. Sci.* **2011**, *46*, 2821.
- [9] a) K. Nanjundaswamy, A. Padhi, J. Goodenough, S. Okada, H. Ohtsuka, H. Arai, J. Yamaki, *Solid State Ionics* **1996**, *92*, 1; b) J.-Z. Sun, *Asian. J. Chem.* **2010**, *22*, 260; c) K. Makino, Y. Katayama, T. Miura, T. Kishi, *J. Power Sources* **2001**, *99*, 66.
- [10] A. Nadiri, C. Delmas, R. Salmon, P. Hagenmuller, *Rev. Chim. Minérale* **1984**, *21*, 537.
- [11] W. Reiff, J. Zhang, C. Torardi, *J. Solid State Chem.* **1986**, *62*, 231.
- [12] C. Torardi, E. Prince, *Mater. Res. Bull.* **1986**, *21*, 719.
- [13] A. Manthiram, J. Goodenough, *J. Solid State Chem.* **1987**, *71*, 349.
- [14] A. Manthiram, J. Goodenough, *J. Power Sources* **1989**, *26*, 403.
- [15] S. Okada, K. Nanjundaswamy, A. Manthiram, J. Goodenough, H. Ohtsuka, H. Arai, J. Yamaki, presented at *36th Power Sources Conf.*, June **1994**.
- [16] C. Masquelier, A. Padhi, K. Nanjundaswamy, J. Goodenough, *J. Solid State Chem.* **1998**, *135*, 228.
- [17] M. Morcrette, C. Wurm, C. Masquelier, *Solid State Sci.* **2002**, *4*, 239.
- [18] A. Padhi, V. Manivannan, J. Goodenough, *J. Electrochem. Soc.* **1998**, *145*, 1518.
- [19] P. Bruce, G. Miln, *J. Solid State Chem.* **1990**, *89*, 162.
- [20] Q. Sun, Q.-Q. Ren, Z.-W. Fu, *Electrochim. Commun.* **2012**, *23*, 145.
- [21] a) V. Nguyen, Y. Liu, X. Yang, W. Chen, *ECS Electrochem. Lett.* **2015**, *4*, A29; b) V. Nguyen, Y. Liu, Y. Li, S. A. Hakim, X. Yang, W. Chen, *ECS J. Solid State Sci. Technol.* **2015**, *4*, M25; c) V. Nguyen, Y. Liu, S. A. Hakim, S. Yang, A. R. Radwan, W. Chen, *Int J. Electrochem. Sci.* **2015**, *10*, 10565.
- [22] a) W. Wang, Q. Luo, B. Li, X. Wei, L. Li, Z. Yang, *Adv. Funct. Mater.* **2013**, *23*, 970; b) R. Satish, V. Aravindan, W. C. Ling, S. Madhavi, *J. Power Sources* **2015**, *281*, 310.
- [23] Y. Qiao, X. Wang, Y. Mai, J. Xiang, D. Zhang, C. Gu, J. Tu, *J. Power Sources* **2011**, *196*, 8706.
- [24] a) X. Rui, N. Yesibolati, C. Chen, *J. Power Sources* **2011**, *196*, 2279; b) X. Rui, N. Yesibolati, S. Li, C. Yuan, C. Chen, *Solid State Ionics* **2011**, *187*, 58.
- [25] J. Gaubicher, J. Angenaut, Y. Chabre, T. Le Mercier, M. Quarton, *Mol. Cryst. Liq. Cryst.* **1998**, *311*, 45.
- [26] F. d'Yvoire, M. Pintard-Scrépel, E. Bretey, M. de la Rochere, *Solid State Ionics* **1983**, *9*, 851.
- [27] S.-C. Yin, H. Grondéy, P. Strobel, M. Anne, L. F. Nazar, *J. Am. Chem. Soc.* **2003**, *125*, 10402.
- [28] a) M. Saidi, J. Barker, H. Huang, J. Swoyer, G. Adamson, *J. Power Sources* **2003**, *119*, 266; b) S. Patoux, C. Wurm, M. Morcrette, G. Rousse, C. Masquelier, *J. Power Sources* **2003**, *119*, 278; c) M. Saidi, J. Barker, H. Huang, J. Swoyer, G. Adamson, *Electrochim. Solid-State Lett.* **2002**, *5*, A149.
- [29] a) J. Yoon, S. Muhammad, D. Jang, N. Sivakumar, J. Kim, W.-H. Jang, Y.-S. Lee, Y.-U. Park, K. Kang, W.-S. Yoon, *J. Alloys Compd.* **2013**, *569*, 76; b) H. Huang, S. C. Yin, T. Kerr, N. Taylor, L. F. Nazar, *Adv. Mater.* **2002**, *14*, 1525.

- [30] M. Morcrette, J. Leriche, S. Patoux, C. Wurm, C. Masquelier, *Electrochim. Solid-State Lett.* **2003**, *6*, A80.
- [31] J. Huang, L. Yang, K. Liu, Y. Tang, *J. Power Sources* **2010**, *195*, 5013.
- [32] A. Pan, J. Liu, J.-G. Zhang, W. Xu, G. Cao, Z. Nie, B. W. Arey, S. Liang, *Electrochim. Commun.* **2010**, *12*, 1674.
- [33] H. Liu, G. Yang, X. Zhang, P. Gao, L. Wang, J. Fang, J. Pinto, X. Jiang, *J. Mater. Chem.* **2012**, *22*, 11039.
- [34] a) C. Wang, J. Hong, *Electrochim. Solid-State Lett.* **2007**, *10*, A65; b) P. S. Herle, B. Ellis, N. Coombs, L. Nazar, *Nat. Mater.* **2004**, *3*, 147.
- [35] S.-Y. Chung, J. T. Bloking, Y.-M. Chiang, *Nat. Mater.* **2002**, *1*, 123.
- [36] a) P. Fu, Y. Zhao, Y. Dong, X. An, G. Shen, *J. Power Sources* **2006**, *162*, 651; b) X. Zhou, Y. Liu, Y. Guo, *Electrochim. Acta* **2009**, *54*, 2253; c) P. Fu, Y. Zhao, Y. Dong, X. An, G. Shen, *Electrochim. Acta* **2006**, *52*, 1003; d) Y. Li, X. Liu, J. Yan, *Electrochim. Acta* **2007**, *53*, 474; e) X. Zhu, Y. Liu, L. Geng, L. Chen, H. Liu, M. Cao, *Solid State Ionics* **2008**, *179*, 1679.
- [37] a) T. Jiang, W. Pan, J. Wang, X. Bie, F. Du, Y. Wei, C. Wang, G. Chen, *Electrochim. Acta* **2010**, *55*, 3864; b) Y. Li, Z. Zhou, M. Ren, X. Gao, J. Yan, *Electrochim. Acta* **2006**, *51*, 6498; c) Y. Li, Z. Zhou, X. Gao, J. Yan, *Electrochim. Acta* **2007**, *52*, 4922; d) X. Rui, C. Li, J. Liu, T. Cheng, C. Chen, *Electrochim. Acta* **2010**, *55*, 6761.
- [38] a) C. Sun, S. Rajasekharan, Y. Dong, J. B. Goodenough, *ACS Appl. Mater. Interfaces* **2011**, *3*, 3772; b) Y. Qiao, J. Tu, X. Wang, C. Gu, *J. Power Sources* **2012**, *199*, 287; c) C. Wang, H. Liu, W. Yang, *J. Mater. Chem.* **2012**, *22*, 5281; d) K. Nathiya, D. Bhuvaneswari, N. Kalaiselvi, *Mater. Res. Bull.* **2012**, *47*, 4300; e) X. Du, W. He, X. Zhang, Y. Yue, H. Liu, X. Zhang, D. Min, X. Ge, Y. Du, *J. Mater. Chem.* **2012**, *22*, 5960.
- [39] W. Duan, Z. Hu, K. Zhang, F. Cheng, Z. Tao, J. Chen, *Nanoscale* **2013**, *5*, 6485.
- [40] Q. Chen, T. Zhang, X. Qiao, D. Li, J. Yang, *J. Power Sources* **2013**, *234*, 197.
- [41] X. Rui, D. Sim, K. Wong, J. Zhu, W. Liu, C. Xu, H. Tan, N. Xiao, H. H. Hng, T. M. Lim, *J. Power Sources* **2012**, *214*, 171.
- [42] Q. Wei, Q. An, D. Chen, L. Mai, S. Chen, Y. Zhao, K. M. Hercule, L. Xu, A. Minhas-Khan, Q. Zhang, *Nano Lett.* **2014**, *14*, 1042.
- [43] Q. Kuang, Y. Zhao, Z. Liang, *J. Power Sources* **2011**, *196*, 10169.
- [44] C. Dai, Z. Chen, H. Jin, X. Hu, *J. Power Sources* **2010**, *195*, 5775.
- [45] W.-l. Wu, J. Liang, J. Yan, W.-f. Mao, *J. Solid State Electrochem.* **2013**, *17*, 2027.
- [46] a) J. Son, G. Kim, M. Kim, S. Kim, V. Aravindan, Y. Lee, *J. Electrochem. Soc.* **2013**, *160*, A87; b) A. Cho, J. Son, V. Aravindan, H. Kim, K. Kang, W. Yoon, W. Kim, Y. Lee, *J. Mater. Chem.* **2012**, *22*, 6556.
- [47] Y. Chen, Y. Zhao, X. An, J. Liu, Y. Dong, L. Chen, *Electrochim. Acta* **2009**, *54*, 5844.
- [48] C. Deng, S. Zhang, S. Yang, Y. Gao, B. Wu, L. Ma, B. Fu, Q. Wu, F. Liu, *J. Phys. Chem. C* **2011**, *115*, 15048.
- [49] M. Sato, H. Ohkawa, K. Yoshida, M. Saito, K. Uematsu, K. Toda, *Solid State Ionics* **2000**, *135*, 137.
- [50] W. Yuan, J. Yan, Z. Tang, O. Sha, J. Wang, W. Mao, L. Ma, *Electrochim. Acta* **2012**, *72*, 138.
- [51] E. Kobayashi, L. S. Plashnitsa, T. Doi, S. Okada, J.-I. Yamaki, *Electrochim. Commun.* **2010**, *12*, 894.
- [52] W.-F. Mao, H.-Q. Tang, Z.-Y. Tang, J. Yan, Q. Xu, *ECS Electrochem. Lett.* **2013**, *2*, A69.
- [53] a) J. Gaubicher, C. Wurm, G. Goward, C. Masquelier, L. Nazar, *Chem. Mater.* **2000**, *12*, 3240; b) C. M. Burba, R. Frech, *Solid State Ionics* **2007**, *177*, 3445.
- [54] B. L. Cushing, J. B. Goodenough, *J. Solid State Chem.* **2001**, *162*, 176.
- [55] Y. Lu, L. Wang, J. Song, D. Zhang, M. Xu, J. B. Goodenough, *J. Mater. Chem. A* **2013**, *1*, 68.
- [56] Z. Jian, W. Han, Y. Liang, Y. Lan, Z. Fang, Y.-S. Hu, Y. Yao, *J. Mater. Chem. A* **2014**, *2*, 20231.
- [57] a) L. S. Plashnitsa, E. Kobayashi, Y. Noguchi, S. Okada, J.-I. Yamaki, *J. Electrochim. Soc.* **2010**, *157*, A536; b) Z. Jian, L. Zhao, H. Pan, Y.-S. Hu, H. Li, W. Chen, L. Chen, *Electrochim. Commun.* **2012**, *14*, 86.
- [58] a) J. Gopalakrishnan, K. K. Rangan, *Chem. Mater.* **1992**, *4*, 745; b) S. Y. Lim, H. Kim, R. Shakoor, Y. Jung, J. W. Choi, *J. Electrochim. Soc.* **2012**, *159*, A1393; c) Y. H. Jung, C. H. Lim, D. K. Kim, *J. Mater. Chem. A* **2013**, *1*, 11350.
- [59] C. Delmas, R. Olazcuaga, F. Cherkaoui, R. Brochu, G. Leflem, *C. R. Seances Acad. Sci. Ser. C* **1978**, *287*, 169.
- [60] Z. Jian, C. Yuan, W. Han, X. Lu, L. Gu, X. Xi, Y. S. Hu, H. Li, W. Chen, D. F. Chen, Y. Ikuhara, L. Q. Chen, *Adv. Funct. Mater.* **2014**, *24*, 4265.
- [61] J.-N. Chotard, G. Rousse, R. David, O. Mentré, M. Courty, C. Masquelier, *Chem. Mater.* **2015**, *27*, 5982.
- [62] a) W. Shen, C. Wang, H. Liu, W. Yang, *Chem.–Eur. J.* **2013**, *19*, 14712; b) C. Zhu, K. Song, P. A. van Aken, J. Maier, Y. Yu, *Nano Lett.* **2014**, *14*, 2175.
- [63] Z. Jian, Y. Sun, X. Ji, *Chem. Commun.* **2015**, *51*, 6381.
- [64] Z. Jian, W. Han, X. Lu, H. Yang, Y. S. Hu, J. Zhou, Z. Zhou, J. Li, W. Chen, D. F. Chen, L. Q. Chen, *Adv. Energy Mater.* **2013**, *3*, 156.
- [65] W. Song, X. Cao, Z. Wu, J. Chen, K. Huangfu, X. Wang, Y. Huang, X. Ji, *Phys. Chem. Chem. Phys.* **2014**, *16*, 17681.
- [66] A. K. Padhi, K. Nanjundaswamy, J. Goodenough, *J. Electrochim. Soc.* **1997**, *144*, 1188.
- [67] J. H. Gordon, J. J. Watkins, US 20100239893 A1, **2010**.
- [68] a) J. Liu, K. Tang, K. Song, P. A. van Aken, Y. Yu, J. Maier, *Nanoscale* **2014**, *6*, 5081; b) Y. Jiang, Z. Yang, W. Li, L. Zeng, F. Pan, M. Wang, X. Wei, G. Hu, L. Gu, Y. Yu, *Adv. Energy Mater.* **2015**, *5*, 1402104; c) X. Rui, W. Sun, C. Wu, Y. Yu, Q. Yan, *Adv. Mater.* **2015**, *27*, 6670; d) J. Z. Guo, X. L. Wu, F. Wan, J. Wang, X. H. Zhang, R. S. Wang, *Chem.–Eur. J.* **2015**, *21*, 17371.
- [69] K. Saravanan, C. W. Mason, A. Rudola, K. H. Wong, P. Balaya, *Adv. Energy Mater.* **2013**, *3*, 444.
- [70] S. Li, Y. Dong, L. Xu, X. Xu, L. He, L. Mai, *Adv. Mater.* **2014**, *26*, 3545.
- [71] Y. Fang, L. Xiao, X. Ai, Y. Cao, H. Yang, *Adv. Mater.* **2015**, *27*, 5895.
- [72] C. Zhu, P. Kopold, P. A. van Aken, J. Maier, Y. Yu, *Adv. Mater.* **2016**, *28*, 2409.
- [73] W. Duan, Z. Zhu, H. Li, Z. Hu, K. Zhang, F. Cheng, J. Chen, *J. Mater. Chem. A* **2014**, *2*, 8668.
- [74] Z. Jian, V. Raju, Z. Li, Z. Xing, Y. S. Hu, X. Ji, *Adv. Funct. Mater.* **2015**, *25*, 5778.
- [75] Y. Noguchi, E. Kobayashi, L. S. Plashnitsa, S. Okada, J.-I. Yamaki, *Electrochim. Acta* **2013**, *101*, 59.
- [76] F. Lalère, J.-B. Leriche, M. Courty, S. Boulineau, V. Viallet, C. Masquelier, V. Seznec, *J. Power Sources* **2014**, *247*, 975.
- [77] W. Song, X. Ji, Y. Zhu, H. Zhu, F. Li, J. Chen, F. Lu, Y. Yao, C. Banks, *ChemElectroChem* **2014**, *1*, 871.
- [78] a) C. Delmas, A. Nadiri, J. Soubeyroux, *Solid State Ionics* **1988**, *28*, 419; b) C. Delmas, A. Nadiri, *Mater. Res. Bull.* **1988**, *23*, 65.
- [79] a) H. Aono, E. Sugimoto, Y. Sadaoka, N. Imanaka, G. y. Adachi, *J. Electrochim. Soc.* **1990**, *137*, 1023; b) D. Rettenwander, A. Welzl, S. Pristat, F. Tietz, S. Taibl, G. Redhammer, J. Fleig, *J. Mater. Chem. A* **2016**, *4*, 1506; c) A. V. Rao, V. Veeraiah, A. P. Rao, B. K. Babu, M. Brahmayya, *Res. Chem. Intermed.* **2015**, *41*, 4327; d) D. H. Kothari, D. Kanchan, *Ionics* **2015**, *21*, 1253; e) P. Zhang, H. Wang, Q. Si, M. Matsui, Y. Takeda, O. Yamamoto, N. Imanishi, *Solid State Ionics* **2015**, *272*, 101.
- [80] S. Patoux, C. Masquelier, *Chem. Mater.* **2002**, *14*, 5057.
- [81] A. Aatiq, M. Ménétrier, L. Croguennec, E. Suard, C. Delmas, *J. Mater. Chem.* **2002**, *12*, 2971.
- [82] H. Kabbour, D. Coillot, M. Colmont, C. Masquelier, O. Mentré, *J. Am. Chem. Soc.* **2011**, *133*, 11900.

- [83] V. Aravindan, W. Chuiling, M. Reddy, G. S. Rao, B. Chowdari, S. Madhvani, *Phys. Chem. Chem. Phys.* **2012**, *14*, 5808.
- [84] Z. Huang, L. Liu, Q. Zhou, J. Tan, Z. Yan, D. Xia, H. Shu, X. Yang, X. Wang, *J. Power Sources* **2015**, *294*, 650.
- [85] G. Z. Yang, H. W. Song, M. Wu, C. Wang, *J. Mater. Chem. A* **2015**, *3*, 9.
- [86] J. Y. Luo, Y. Y. Xia, *Adv. Funct. Mater.* **2007**, *17*, 3877.
- [87] G. Pang, C. Yuan, P. Nie, B. Ding, J. Zhu, X. Zhang, *Nanoscale* **2014**, *6*, 6328.
- [88] X.-H. Liu, T. Saito, T. Doi, S. Okada, J.-I. Yamaki, *J. Power Sources* **2009**, *189*, 706.
- [89] a) Z. Liu, X. Qin, H. Xu, G. Chen, *J. Power Sources* **2015**, *293*, 562; b) L. Liu, T. Song, H. Han, H. Park, J. Xiang, Z. Liu, Y. Feng, U. Paik, *J. Mater. Chem. A* **2015**, *3*, 10395.
- [90] W. Zhu, F.-G. Niu, Y.-P. Yang, Z.-L. Wang, J. Yao, Z.-G. Wang, *Asian. J. Chem.* **2014**, *26*, 2916.
- [91] a) G. Pang, P. Nie, C. Yuan, L. Shen, X. Zhang, J. Zhu, B. Ding, *Energy Technol.* **2014**, *2*, 705; b) W. Wu, A. Mohamed, J. Whitacre, *J. Electrochem. Soc.* **2013**, *160*, A497; c) W. Wu, S. Shabagh, J. Chang, A. Rutt, J. F. Whitacre, *J. Electrochem. Soc.* **2015**, *162*, A803.
- [92] Y. Wang, L. Mu, J. Liu, Z. Yang, X. Yu, L. Gu, Y. S. Hu, H. Li, X. Q. Yang, L. Chen, *Adv. Energy Mater.* **2015**, *5*, 1501005.
- [93] X. Y. Wu, M. Y. Sun, Y. F. Shen, J. F. Qian, Y. L. Cao, X. P. Ai, H. X. Yang, *ChemSusChem* **2014**, *7*, 407.
- [94] X. Wu, Y. Cao, X. Ai, J. Qian, H. Yang, *Electrochim. Commun.* **2013**, *31*, 145.
- [95] J.-Y. Luo, W.-J. Cui, P. He, Y.-Y. Xia, *Nat. Chem.* **2010**, *2*, 760.
- [96] D. Sun, X. Xue, Y. Tang, Y. Jing, B. Huang, Y. Ren, Y. Yao, H. Wang, G. Cao, *ACS Appl. Mater. Interfaces* **2015**, *7*, 28337.
- [97] S. I. Park, I. Gocheva, S. Okada, J.-I. Yamaki, *J. Electrochim. Soc.* **2011**, *158*, A1067.
- [98] Z. Li, D. Young, K. Xiang, W. C. Carter, Y. M. Chiang, *Adv. Energy Mater.* **2013**, *3*, 290.
- [99] W. Wu, J. Yan, A. Wise, A. Rutt, J. Whitacre, *J. Electrochim. Soc.* **2014**, *161*, A561.
- [100] W. Zhou, H. Gao, J. B. Goodenough, *Adv. Energy Mater.* **2016**, *6*, 1501802.
- [101] a) H.-K. Roh, H.-K. Kim, K. C. Roh, K.-B. Kim, *RSC Adv.* **2014**, *4*, 31672; b) Y. Wang, J. Yi, Y. Xia, *Adv. Energy Mater.* **2012**, *2*, 830.
- [102] P. Senguttuvan, G. Rousse, M. Arroyo y de Dompablo, H. Vezin, J.-M. Tarascon, M. Palacín, *J. Am. Chem. Soc.* **2013**, *135*, 3897.
- [103] A. Padhi, K. Nanjundaswamy, C. Masquelier, J. Goodenough, *J. Electrochim. Soc.* **1997**, *144*, 2581.
- [104] S. Patoux, G. Rousse, J.-B. Leriche, C. Masquelier, *Chem. Mater.* **2003**, *15*, 2084.
- [105] a) O. Tillement, J. Angenault, J. Couturier, M. Quarton, *Solid State Ionics* **1991**, *44*, 299; b) O. Tillement, J. Angenault, J. Couturier, M. Quarton, *Solid State Ionics* **1992**, *53*, 391; c) O. Tillement, J. Couturier, J. Angenault, M. Quarton, *Solid State Ionics* **1991**, *48*, 249.
- [106] C. Wu, P. Kopold, Y.-L. Ding, P. A. van Aken, J. Maier, Y. Yu, *ACS Nano* **2015**, *9*, 6610.
- [107] K. B. Hueso, M. Armand, T. Rojo, *Energy Environ. Sci.* **2013**, *6*, 734.
- [108] a) O. Bohnke, S. Ronchetti, D. Mazza, *Solid State Ionics* **1999**, *122*, 127; b) S. Baliteau, A. Sauvet, C. Lopez, P. Fabry, *J. Eur. Ceram. Soc.* **2005**, *25*, 2965.
- [109] Z. Z. Zhang, S. Q. Si, Y.-S. Hu, L. Q. Chen, *J. Inorg. Mater.* **2013**, *28*, 1255.
- [110] J.-K. Kim, Y. J. Lim, H. Kim, G.-B. Cho, Y. Kim, *Energy Environ. Sci.* **2015**, *8*, 3589.
- [111] T. Asai, K. Ado, Y. Saito, H. Kageyama, O. Nakamura, *Solid State Ionics* **1989**, *35*, 319.
- [112] T. Hashimoto, K. Hayashi, *Electrochim. Acta* **2015**, *182*, 809.
- [113] K. Hayashi, K. Shima, F. Sugiyama, *J. Electrochem. Soc.* **2013**, *160*, A1467.
- [114] H. Schmid, L. C. De Jonghe, C. Cameron, *Solid State Ionics* **1982**, *6*, 57.
- [115] a) J. Kuwano, N. Sato, M. Kato, K. Takano, *Solid State Ionics* **1994**, *70*, 332; b) S.-C. Li, Z.-X. Lin, *Solid State Ionics* **1983**, *9*, 835; c) K. Arbi, M. Lazarraga, D. Ben Hassen Chehimi, M. Ayadi-Trabelsi, J. Rojo, J. Sanz, *Chem. Mater.* **2004**, *16*, 255.
- [116] a) A. Svitán'ko, S. Novikova, D. Safronov, A. Yaroslavtsev, *Inorg. Mater.* **2011**, *47*, 1391; b) M. Subramanian, R. Subramanian, A. Clearfield, *Solid State Ionics* **1986**, *18*, 562; c) H. Aono, E. Sugimoto, Y. Sadaoka, N. Imanaka, G. y. Adachi, *J. Electrochim. Soc.* **1989**, *136*, 590; d) Y. O. Korepin, L. S. Bigeeva, A. Il'in, A. Svitán'ko, S. Novikova, A. Yaroslavtsev, *Inorg. Mater.* **2013**, *49*, 283.
- [117] a) I. Y. Pinus, I. Arkhangel'skii, N. Zhuravlev, A. Yaroslavtsev, *Rus. J. Inorg. Chem.* **2009**, *54*, 1173; b) A. Svitán'ko, S. Novikova, I. Stenina, V. Skopets, A. Yaroslavtsev, *Inorg. Mater.* **2014**, *50*, 273.
- [118] a) Z.-X. Lin, H.-J. Yu, S.-C. Li, S.-B. Tian, *Solid State Ionics* **1988**, *31*, 91; b) H. Aono, E. Sugimoto, Y. Sadaoka, N. Imanaka, G.-y. Adachi, *Solid State Ionics* **1993**, *62*, 309.
- [119] a) H. Hosono, Y. Abe, *J. Am. Ceram. Soc.* **1992**, *75*, 2862; b) K. Arbi, J. Rojo, J. Sanz, *J. Eur. Ceram. Soc.* **2007**, *27*, 4215.
- [120] C. Vidal-Abarca, P. Lavela, M. Aragón, N. Plylahan, J. Tirado, *J. Mater. Chem.* **2012**, *22*, 21602.
- [121] M. Kotobuki, M. Koishi, Y. Kato, *Ionics* **2013**, *19*, 1945.
- [122] K. Arbi, W. Bucheli, R. Jiménez, J. Sanz, *J. Eur. Ceram. Soc.* **2015**, *35*, 1477.
- [123] Y. Iriyama, C. Yada, T. Abe, Z. Ogumi, K. Kikuchi, *Electrochim. Commun.* **2006**, *8*, 1287.
- [124] P. Birke, F. Salam, S. Döring, W. Weppner, *Solid State Ionics* **1999**, *118*, 149.
- [125] Y. Inda, T. Katoh, M. Baba, *J. Power Sources* **2007**, *174*, 741.
- [126] a) J. Xie, N. Imanishi, T. Zhang, A. Hirano, Y. Takeda, O. Yamamoto, *J. Power Sources* **2009**, *189*, 365; b) J. Kumar, S. J. Rodrigues, B. Kumar, *J. Power Sources* **2010**, *195*, 327; c) M. Rosso, T. Gobron, C. Brissot, J.-N. Chazalviel, S. Lascaud, *J. Power Sources* **2001**, *97*, 804; d) S. Liu, N. Imanishi, T. Zhang, A. Hirano, Y. Takeda, O. Yamamoto, J. Yang, *J. Electrochim. Soc.* **2010**, *157*, A1092.
- [127] a) J. Xie, N. Imanishi, T. Zhang, A. Hirano, Y. Takeda, O. Yamamoto, *J. Power Sources* **2009**, *192*, 689; b) J. Xie, N. Imanishi, T. Zhang, A. Hirano, Y. Takeda, O. Yamamoto, *J. Power Sources* **2010**, *195*, 5780; c) J. Xie, N. Imanishi, T. Zhang, A. Hirano, Y. Takeda, O. Yamamoto, X. Zhao, G. Cao, *J. Power Sources* **2010**, *195*, 8341.
- [128] B. Kumar, J. Kumar, R. Leese, J. P. Fellner, S. J. Rodrigues, K. Abraham, *J. Electrochim. Soc.* **2010**, *157*, A50.
- [129] H. Kitaura, H. Zhou, *Energy Environ. Sci.* **2012**, *5*, 9077.
- [130] a) T. Zhang, N. Imanishi, S. Hasegawa, A. Hirano, J. Xie, Y. Takeda, O. Yamamoto, N. Sammes, *J. Electrochim. Soc.* **2008**, *155*, A965; b) S. Hasegawa, N. Imanishi, T. Zhang, J. Xie, A. Hirano, Y. Takeda, O. Yamamoto, *J. Power Sources* **2009**, *189*, 371; c) Y. Wang, H. Zhou, *J. Power Sources* **2010**, *195*, 358; d) L. Li, X. Zhao, A. Manthiram, *Electrochim. Commun.* **2012**, *14*, 78.
- [131] H. Li, Y. Wang, H. Na, H. Liu, H. Zhou, *J. Am. Chem. Soc.* **2009**, *131*, 15098.
- [132] T. Zhang, H. Zhou, *Nat. Commun.* **2013**, *4*, 1817.
- [133] Y. Ding, G. H. Yu, *Angew. Chem., Int. Ed.* **2016**, *55*, 4772.
- [134] L. Li, S.-H. Chai, S. Dai, A. Manthiram, *Energy Environ. Sci.* **2014**, *7*, 2630.